Discriminating between the roles of Late Pleistocene palaeodischarge and geological-topographic inheritance in fluvial longitudinal profile and channel development

Discriminating between the roles of Late Pleistocene palaeodischarge and geological-topographic inheritance in fluvial longitudinal profile and channel development.

Colman Gallagher[1,2], Matthew Balme[3,4] and Nicholas Clifford[5]

[1]UCD School of Geography, University College Dublin, Belfield, Dublin D04 V1W8, Ireland.

[2]UCD Earth Institute, University College Dublin, Belfield, Dublin D04 V1W8, Ireland.

colman.gallagher@ucd.ie

[2]Dept. of Physical Sciences, Open University, Walton Hall, Milton Keynes MK7 6AA, UK.

[3]Planetary Science Institute Tucson, 1700 E. Fort Lowell, Suite 106, Tucson, AZ 85719, United States.

[5]School of Social, Political and Geographical Sciences, Loughborough University, Loughborough, LE11 3TU. UK.

KEY WORDS

Quaternary geomorphology, long profile pool-sequence, palaeodischarge, relative sea level, landscape evolution.

ABSTRACT

This paper investigates the influences of palaeohydrology and geological-topographic inheritance in shaping the channel of the lower River Suir, southeast Ireland. Results of acoustic surveys of the lower River Suir and Waterford Harbour reveal two scales of pseudo-cyclic river bedforms. Longitudinal elevation profiles of the geological topography (undulating bedrock and till-mantled bedrock) bounding the present floodplain swath reveal pseudo-cyclicity in that terrain too. Spectral and statistical analyses are used to quantify the cyclicity of the long profile and geological-topographic series. These methods show that the dominant cyclicity of the long profile reflects autocorrelation more than inheritance of cyclicity from the bounding geological topography. The cyclicity of the long profile mainly reflects a hydraulic control on pool-spacing, although some cyclicity probably has been inherited from the geological-topography. Channel-forming palaeodischarge is estimated based on the dominant pool-spacing revealed by spectral analysis, validated using relationships between meander wavelength, channel cross-sectional geometry and hydraulically-informed discharge reconstruction. The palaeodischarge estimates are in close agreement and are two orders of magnitude greater than present flood maxima. Significantly, these palaeodischarge estimates also agree closely with palaeodischarge calculated for the submerged Pleistocene palaeochannel that extends across the near-shore continental shelf from Waterford Harbour. The pool-sequence of the lower Suir and the submerged palaeochannel represent a former land-system that was active during a period of low relative sea level during the last glacial. More broadly, the paper offers insights into the landscape evolution of formerly glaciated regions that experienced very wide

discharge variability during and after the transition from glacial to interglacial regimes, in a context of complex relative sea level change.

INTRODUCTION

This paper presents the results and quantitative analyses of acoustic surveys of the long profile (LP) of the lower River Suir, from its tidal limit to its entry into the North Atlantic Ocean through Waterford Harbour, southeastern Ireland (Fig. 1). The goals of the paper are to describe quantitatively the morphometric characteristics of the LP and to explain them in the context of broader Quaternary landscape evolution, including bedrock erosion, glacigenic deposition, palaeohydrology and relative sea level (RSL) change. The key finding of the surveys is that the LP of the lower Suir is characterised by a pseudo-cyclic sequence of pools spaced at >1 km intervals (Fig. 1 and 2). Hence, this paper primarily aims to understand the pool-spacing of the lower Suir as a means of offering insights to the evolution of channel form and the environmental contexts within which process and form evolve. River channel pool-riffle or step-pool sequences are autogenic bedforms (Clifford, 1993) that characterise the long profiles of alluvial, coarse clastic and bedrock channels. Pools are spatially self-organised through the development of discharge-related three-dimensional macroturbulence, variation in channel width, scour and selective sediment transport (de Almeida et al., 2012; Bayat et al., 2014; Morgan and Nelson, 2016). Erosion of bedrock substrates leading to pool development is most intense when protective sediment mantles are stripped in extreme floods (Howard, 1998). Pool-spacing reflects the focusing of scour on geological weaknesses (Wohl, 1998), e.g. transverse fracture zones (Dolan et al., 1978), bedding-planes and joints (e.g. Baker and Pickup, 1987). However, the rate of incision into bedrock also depends on

the extent of bedrock exposure, which is maximised when sediment supply and transport capacity are nearly equal and small increases in shear stress produce large increases in bedrock exposure (Sklar and Dietrich, 2004). Hence, bedrock exposure is very sensitive to the rate and size of sediment supplied to the channel during rock uplift or climate change (both, in a context of glacio-isostatic uplift occurring during deglaciation) when small changes in channel slope can produce changes in the rate of bedrock incision that are both large and more rapid than changes in overall relief (Sklar and Dietrich, 2001). Although pools initially form at exogenically determined locations of weakness (Wohl, 1998), a relationship between longitudinal pool-spacing and discharge, the latter represented morphologically *via* adjustment in channel width (w) (Carlston, 1965), has been observed (e.g. Carling and Orr, 2000), including in pool sequences developed entirely in bedrock and in coarse clastic bed material scoured to bedrock (e.g. Dury, 1970).

Scaling between pool-spacing and discharge

Carling and Orr (2000) concluded that riffle spacing ranges from 3w (where w is mean width) in straight channels with nascent meandering, to 7.5w but converges on ~6w as sinuosity increases. This configuration reflects the path length of longitudinally cyclic macroturbulent eddies (Yalin, 1971, 1977, 1992; Carling and Orr, 2000) and the development of riffles at $2\pi/w$. However, Lisle (1986) found that bars tend to be located w upstream and 3 - 4w downstream of bends or large transient obstructions. Clifford (1993) therefore suggested that riffles develop from the bars and bracket intervening pools. Pool-riffle sequences develop initially from the generation of macroturbulent roller eddies that become fixed upstream and downstream of large flow obstacles (Clifford, 1993). Scour of individual pools within

this pattern generates paired deposition downstream and, consequently, a sequence of alternating pools and riffles. Although the initial obstacles are ultimately eroded, the cyclicity of the pool sequence is fixed autogenetically by the pattern of initial flow perturbations (Clifford, 1993). On this basis, and because of similar dimensional relationships between *w* and both threshold sediment transport and eddy size, Clifford (1993) concluded that modal riffle spacing, which tends towards 3*w*, is probably the most appropriate and fundamental scaling relationship. Such relationships between pool-spacing and formative discharge provide a prediction of the pool-spacing of the lower Suir under present-day conditions.

The maximum annual discharge (*Q*) of the Suir in the period 1953 – 2014 was 389 $m^3.s^{-1}$ (OPW, 2016). Empirical relations between *w* and *Q* range from $w = 2.95Q^{0.47}$ (Carlston, 1965) to $w = 4.47Q^{0.5}$ Kellerhals and Church (1989). Therefore, with pool-spacing ranging between 3*w* and 6*w* (Clifford, 1993; Carling and Orr, 2000), the predicted pool-spacing range of the Suir is 94 – 292 m. This range provides the comparative benchmark for the pool-spacing measured in the acoustic surveys for this paper, and both can be assessed against several commonly-used indices that relate channel morphometry to formative discharge, as detailed in Table 1. In this context, the pool-spacing of the lower Suir is one to two orders of magnitude too large to be explained by present-day discharges and, consequently, alternate genetic hypotheses are required.

Alternate hypotheses – palaeodischarge and geological-topographic inheritance

Gallagher (2002) and Gallagher et al. (2004) found that a ~4 km-wide submerged glaciofluvial palaeochannel extends directly from Waterford Harbour for >10 km onto

the continental shelf, before bisecting a submerged complex of morainic boulder ridges in water depths of >56 m. This landform assemblage represents large (up to 10^4 $m^3.s^{-1}$) glaciofluvial discharges from the interior of Ireland to an ice margin located on the Irish continental shelf, during an interval of low relative sea level in the last glacial (Gallagher et al., 2015). While the >1 km-scale pool-sequence of the lower Suir is too large to reflect present-day discharges, it may, then, be consistent in scale with formation by discharges of the same high magnitude as those responsible for the incision of the submerged palaeochannel. However, the non-fluvial geological topography bounding the lower Suir (Fig. 1 and 2) also is characterised by low pseudo-cyclic undulations. This undulating topography is the morphological expression of the densely-faulted, glacially-eroded and thinly till-mantled bedrock substrate (Fig. 1) of the lower Suir valley. The undulations could be imprinted in, and perhaps responsible for (or contribute to) the cyclicity of pool development along the river.

Research strategy

This paper examines the cyclicity of the LP and the contextual geological topography by reference to power spectrum, auto-correlation, cross-correlation and Granger causation analyses. These analyses focus on quantifying the dominant cyclic properties of the LP and the bounding geological topography to discriminate between the contributions of Pleistocene palaeodischarge and geological-topographic inheritance in LP development. Considering the analyses of the lower Suir within the sea level and palaeodischarge context of the submerged extension of Waterford Harbour allows the onshore and offshore channels to be viewed as a coherent Late Quaternary landsystem, providing a new perspective on regional Quaternary

landscape evolution but also offering deeper systematic insights to the origins and evolution of river form across the Pleistocene-Holocene transition. Consequently, new insights are made concerning the interactions between glaciofluvial hydrology, geological-topographic inheritance, glacio-isostatic adjustment (GIA) and RSL change in glacial-transitional and post-glacial landscape development. These insights can be widely applied to developing a better understanding of spatial and temporal variation in the responses of river systems to Quaternary environmental change.

Fig. 1 here

STUDY REACH AND PALAEOENVIRONMENTAL CONTEXT

The River Suir drains a catchment of 3542 km^2 and is tidal to Carrick-on-Suir (Fig. 1). Between 1953 and 2014 its annual maximum discharge averaged 222 m^3s^{-1} (OPW, 2016). Maximum and mean annual discharges in the period 1940 – 2005 were 389 m^3s^{-1} and 45 m^3s^{-1}. Maximum flood discharge through Waterford Harbour, following confluence with discharge from the Barrow-Nore system, is significantly less than 1000 $m^3.s^{-1}$.

The rivers of southern Ireland are incised into uplands in the form of Lower Palaeozoic metasedimentary inliers and lowlands dominated by Carboniferous limestones that occupy broad synclinal troughs aligned east-west along the Variscan trend. The upper reaches of the lower Suir closely follow the contact between a low-lying Carboniferous limestone basin on the north and flanking hills of Lower Palaeozoic metasediments and volcanics on the south (Fig. 1). Hence, the river here

is topographically constricted to the south but less confined to the north. The lowermost reaches of the lower Suir are incised into more heterogeneous and more constricting terrain, crossing through formations of Ordovician metasediments and volcanics that overlook the limestone trough to the north and west (Fig. 1). Closely-spaced (<1 km to ~5 km) tensional faults strike broadly NNW-SSE through the Lower Palaeozoic rocks of the lower Suir catchment, the limestones having also developed karst terrain following stripping of Mesozoic cover rocks during the Tertiary (Clarke et al., 2007). In the Pleistocene, the bedrock floor of the lower Suir valley was glacially scoured and then thinly and discontinuously mantled by tills (e.g. Parkes and Meehan, 2012). The pattern of NNW-SSE faults striking through glacially-scoured bedrock, thinly mantled by till, probably accounts for the present undulatory geological topography bounding the lower Suir. The tills are dominated petrographically by transported clasts of Carboniferous limestone. The valley sides are characterised either by till dominated by transported clasts of Devonian sandstone or by glacially abraded bedrock within 1 m of the surface (Hegarty, 2004; GSI, 2015c). Glaciofluvial channels, terraces, sands and gravels occur extensively across the Suir valley only above the present tidal limit. However, large engineering projects have revealed that the channel of the lower Suir is underlain by glaciofluvial deposits, up to 20 m thick, of clayey sands, gravels and boulders (Phillips et al., 2012). All Pleistocene glacigenic deposits in southeastern Ireland were laid down in the last glaciation (Warren, 1985; Gallagher and Thorp, 1997; Hegarty, 2004; O'Cofaigh et al., 2012; Gallagher et al., 2015) during Marine Isotope Stage (MIS) 2 (Lisiecki and Raymo, 2005: MIS 2, 14-29 ka; MIS 3, 29-57 ka; MIS 4, 57-71 ka). The glaciofluvial landforms of the Suir valley indicate that it was an arterial conduit for glacial meltwaters (Orme, 1964), which became confluent in Waterford Harbour with

glaciofluvial discharges from the Barrow and Nore valleys (Warren and Ashley, 1984; Gallagher, 2002; Gallagher et al., 2004; Hegarty, 2004). Together with bedrock pinch-points, the distribution of till and glaciofluvial deposits accounts for the overall slope, meander belt potential and both the morphological and geotechnical variability of the valley (e.g. rock *v* sediment-mantled and diamicton *v* stratified reaches). These factors are crucial to understanding valley and river channel evolution in southeastern Ireland, essentially suggesting the importance of longer-term geological-climatic inheritance as a backdrop to more recent landform morphodynamics.

The catchments of the Rivers Suir, Barrow and Nore are contiguous and ultimately confluent through Waterford Harbour (Fig. 1). Gallagher (2002) presented geophysical evidence of the extension of this system onto the continental shelf beyond Waterford Harbour in the form of a large, submerged palaeochannel incised by discharges two orders of magnitude greater than present maximum discharges and adjusted to sea level at least 56 m lower than present (Fig. 1). The response of RSL to glaciation in Ireland, including across its continental shelf (Scourse et al., 2009), was regionally and temporally complex due to GIA (Lambeck, 1993a, 1993b; Bradley et al., 2009; Brooks et al., 2011). Consequently, the hydraulic geometries of terrestrial glaciofluvial channels that developed within existing river valleys have been affected by both the magnitude of glaciofluvial discharge and variation in RSL (Gallagher, 2002; Gallagher et al., 2004). Underwater video imaging showed that the Waterford Harbour palaeochannel terminates at a complex of arcuate boulder ridges Gallagher et al. (2004). This complex was interpreted as a moraine or glacimarine morainal bank that became submerged as ice retreated and RSL rose, flooding

Waterford Harbour to an elevation close to present sea level (Gallagher et al., 2004). The subsequent glacial limit stabilised above the new RSL and is represented by the southernmost extent of the Blackhall Till (Culleton, 1978). The Blackhall Till succeeds dated units of the Courtmacsherry Formation raised beach (Gallagher et al., 2015) and, therefore, was deposited in MIS 2. Hence, the Blackhall Till represents the earliest regional ice margin to have stabilised above the high RSL following the Last Glacial Maximum (LGM). However, the till limit does not intercept the mouth of Waterford Harbour but outcrops only north of the Duncannon Bar (Fig. 1). The LP investigated in this paper extends inland from this limit and the relationship between the LP, the Blackhall Till/Duncannon Bar limit and the earlier submerged palaeochannel is significant in the forthcoming interpretation and palaeoenvironmental contextualisation of the research results.

DATASETS AND METHODOLOGY

Long profile morphometric survey

Depth sounding of the lower Suir, from its tidal limit to the sea off Hook Head (Fig. 1 and 2) was done in two surveys on 30/08/2008 from a rigid-hull inflatable boat (RIB), using an *Eagle Seacharter 480DF* dual frequency echo sounder with an integral GPS. The RIB surveys were done at low tide slack water, aiming to reach the up-river destination at its specific time of low tide (online Appendix, Section A). The average speed of the RIB was 7.9 $m.s^{-1}$ (28 $km.h^{-1}$) with 1 depth sounding per second (7.9 m spatial interval).

Sub-bottom profiling and depth sounding of the lower Suir from the sea to Waterford City were completed between July 2000 and June 2002, aboard the Irish Marine

Institute Research Vessel (RV) *Celtic Voyager*, using a *GeoAcoustics GeoChirp* operating at 1.5 - 11.5 kHz (Gallagher, 2002; Gallagher et al., 2004). Multibeam bathymetry of Waterford Harbour (Fig. 1) and the lower Suir, to Waterford City (Fig. 2), was completed by the Geological Survey of Ireland (GSI) using a *Kongsberg Simrad EM3002* multibeam echosounder aboard the *RV Keary* and a *SEA Swath* interferometric mapping system aboard the *RV Geo* in 2011 (GSI, 2011a and b). Hydrographic data were vertically levelled to Lowest Astronomical Tide (LAT) as described in GSI (2011a and b).

Overlap between the RIB datasets, and comparison with overlapping tidally-corrected GSI multibeam data, showed both excellent replication of results with respect to the location and resolution of bedforms and that the variation in depth between the low tide slack water RIB survey runs and the GSI multibeam dataset corrected to LAT was constant (Fig. 2). The GIS constructed to analyse the data included the EU-DEM (2014) 25 m per pixel topographic dataset and the GSI bedrock 1:100,000 series (GSI, 2015b) and Quaternary (including depth to bedrock) mapping data (GSI, 2015c).

The focus of this research is on the LP of the Suir but also relies on analysis of geological-topographic profiles of bounding non-fluvial materials ca. 1 km south (TPS) and north (TPN) of the channel. The final three elevation profiles used in the analyses (LP, TPS, TPN) were generated within the GIS. Elevation values were extracted at 50 m intervals (hence, LP = 765, TPS = 807 and TPN = 752 measures). TPS and TPN were generated from corridors 500 m wide, as explained in the online Appendix, Section B.

Data analysis

Pseudo-cyclic variation of bed elevation in rivers characterised by pool-sequences has long been studied using autocorrelation and spectral methods (e.g. Richards, 1976). These provide objective means of determining the presence (*versus* a random elevation series) and dimensional characteristics of cyclical topographic components in the profiles. These methods are employed, with some additional variants to add further rigour, in this paper. The PAleontological Statistics (PAST) software package (Hammer et al., 2001) was used for trend testing, spectral, autocorrelation function (ACF) and cross correlation function (CCF) analyses of LP, TPS and TPN. The R code of Wessa (2016) was used for the partial autocorrelation function (PACF) and Granger causality analyses of LP, TPS and TPN. A summary of the analytical steps follows; a full description is given in the online Appendix, Section C.

1) Determination and analysis of cyclicity within and between the LP and geological-topographic profiles (TPS and TPN) required that the profiles LP, TPS and TPN were made statistically stationary by detrending each profile by two degrees of differencing (d =1 and d=2) by serial subtraction. A Mann-Kendall (M-K) trend test (Mann, 1945; Kendall, 1975; Gilbert, 1987) was applied to each detrended series to assess remaining trend following each differencing (Appendix Table A1).
2) The non-parametric Runs Test (RT) about the mean (Wald and Wolfowitz, 1940) was used to test for autocorrelation (indicative of cyclicity) in the raw and detrended series. Statistically significant autocorrelation, therefore

cyclicity, was confirmed in the d = 1 elevation series of dLP, dTPS, dTPN and in the d = 2 elevation series of dTPS and dTPN (Appendix Table A2).

3) Having confirmed autocorrelation, the ACF and PACF of each series (d = 1 and d = 2 for LP, TPS and TPN) were generated. This step confirmed that the differenced series (d = 1 and d = 2) quickly settled to steadily diminishing autocorrelations up to *n*/4 lags, where each lag = 50 m (Box and Jenkins, 1970) and *n* is the total number of data points in each series.
4) The power spectra of the detrended, equally-spaced elevation series (dLP, dTPS dTPN) were determined by generating (i) a Fast Fourier Transform (FFT) to produce graphical models of the cyclic elements of the elevation series and (ii) a Lomb periodogram to determine the peak frequency (*f*), a measure of the rate of recurrence of cyclic elements, equivalent to the lag spacing of highly autocorrelated components. In dLp, dTPS and dTPN, (1/*f*) *lag* provides the physical scale of each significant cyclic component in the LP, TPS and TPN. Both *p*(random), the probability of the power spectrum of the detrended series being random, and the power level that must be exceeded for the significance of frequency peaks in the spectrum to exceed the critical probability levels of $p < 0.05$ and $p < 0.01$ were calculated. Power is expressed as a non-dimensional multiple of unit average power (i.e. = 1).
5) Having identified the significant cyclic characteristics of the detrended elevation series in both the spatial and frequency domains, the statistical associations between the cyclicity of dLP/dTPS (x, y) and dLP/dTPN (x, z) were determined by measuring the CCF of each series pair. The CCFs are interpreted by reference to the ACFs and the power spectra. The analysis

includes a t-Test (Student, 1908) p-value of the CCF, the null hypothesis being that the components in each cross-correlated pair (dTPS/dLP and dTPN/dLP) are samples of the same population. CCF data require pre-whitening, hence the elevation series produced by the second differencing (d = 2) were used. To aid in the interpretation of the d = 2 CCFs as descriptions of physical associations in the landscape, CCFs of the d = 1 associations are also shown.

6) To determine if the elevation series dLP (d = 1 and d = 2) is independent or better predicted by both its own history (ACF) and the history (ACF) of TPS and/or TPN, Granger causality tests were performed on paired combinations of LP, TPS and TPN (Table 2). The tests were applied to both d = 1 and d = 2, as in the power spectrum analysis (for a subsidiary test between meanders 10-16 only d = 1 was used; Fig. 2, Table 2). ACF and CCF plots provide a graphical equivalent of the t-Test. The ACF and CCF plots show the along-series structure of the strength of the serial relationships both internally (ACF) and from one to the other (CCF). Conclusions from Granger-causality tests take the form of "If $y = f(x)$ is statistically significantly, x contains useful information that helps to predict future values of y". In all the tests, the null hypothesis (H_0) of no Granger causality was tested by calculating the critical F statistic with n-1 degrees of freedom. If $F_{calculated} < F_{critical}$, H_0 cannot be rejected and Granger causality is not indicated.

Palaeodischarge, pool-spacing and related morphometry

Estimating channel width and discharge from pool-spacing

Equations (Eqn) 1, 2 and 3 (Table 1) describe the quantitative relations between pool-spacing (S_p), channel width (w), water surface (or bed) slope (S) and discharge (Q). Originating from the determination of the peak pool-spacing from the power spectrum analysis, these relations provide several estimates of discharge. To validate these estimates, palaeodischarge range was estimated from independent measures of channel morphometry and observed bed sediment calibre.

Variable	Relation	Reference	Note
Pool-spacing	$S_p = 3w$ (Eqn 1)	Clifford, 1993; Carling and Orr, 2000	w is channel width.
	$S_p = 7.5w$ (Eqn 2)	Carling and Orr, 2000	
Mean discharge	$Q_m = 0.0227 w_b^{1.71}$ (Eqn 3)	Osterkamp and Hedman (1982)	S is channel bed slope (proxy for palaeo-water surface).
	$Q_m = 0.0074 w_b^{1.54} S^{-0.26}$ (Eqn 4)	Osterkamp and Hedman (1982)	
Bankfull discharge	$Q_{bf} = 4A^{1.21} S^{0.28}$ (Eqn 5)	Williams (1978)	A is bankfull channel cross-sectional area.
	$Q_{bf} = (L_m/32.857)^{1.81}$ (Eqn 6)	Dury (1976)	Uncertainty ± 25%.
Discharge, recurrence interval = 1.5 years	$Q_{1.5} = 0.011 L_m^{1.54}$ (Eqn 7)	Williams (1984)	L_m is meander wavelength.
Manning's roughness coefficient	$n = 0.0926R^{1/6}/1.16 + 2\log_{10}(R/d_{84})$ (Eqn 8)		Inputs in feet. d_{84} = 84th percentile particle size (mm) (Limerinos, 1970).
Critical velocity	$V_{cr} = R^{2/3}S^{0.5}/n$ (Eqn 9)	Manning	R is hydraulic radius, n Manning's roughness coefficient. $R = A/P_w$, (P_w is wetted perimeter from GIS-extracted channel cross-sections, (Fig. 3). Estimated n = 0.05, 0.03, 0.01 (Acrement, 1989), validated with Eqn 8.
	$V_{cr} = 0.18d^{0.49}$ (Eqn 10)	(Costa, 1983)	d = 250 mm, maximum applicable particle diameter but consistent with observed coarse fraction of

			channel forming sediments.
Instantaneous discharge	$Q_i = V_{cr}A$ (Eqn 11)		
Bankfull velocity	$V = Q_{bf}/A$ (Eqn 12)		
Meander wavelength	Lm = 10.23w (Eqn 13)	Soar and Thorne (2001)	
Meander wavelength	Lm = 11.26w to 12.47w (Eqn 14)	Bernard et al. (2007)	Within 95 % confidence limits.

Table 1. Equations used in the estimation of discharge.

Measuring meander wavelength (L_m), sinuosity (s), bankfull channel width (w_b), bankfull cross-sectional area (A) and slope (S) for the calculation of palaeodischarge and validation of palaeodischarge estimates from pool-spacing.

Meander wavelength (L_m) was calculated from the mean value of w_b measured from the GIS (Fig. 2 shows location of cross-sections, Fig. 3 the cross-sections, Table 3 the morphometry). To validate this calculation, L_m was also measured directly from the GIS (Fig. 2, Table 3), based on the co-location of most meander apexes with pools in the RIB sonar LP (see Results section and Fig. 2); meanders were defined as the channel path connecting three consecutive pools, the second in each sequence being at the meander apex. *Lm* was measured as the straight line distance across the meander base between the first and third pool in each sequence. Sinuosity (*s*) was measured from the RIB LP data in the GIS, and classified into channel reaches on the basis of substrate (bedrock type and till or bedrock close to surface).

Bankfull width (w_b) was measured from the EU-DEM topographic layer of the GIS in conjunction with the multibeam sonar bathymetry of the lower Suir, from meander 11 to 16 (Fig. 2d, Table 3). Bankfull channel width (w_b Fig. 3, Table 3) was defined as

the length of the horizontal line segment projected from the lowest major break of slope in the valley profile above present sea level (i.e. 0 m in the cross-sectional profiles) to the opposite bank above which width increased at a greater rate than depth (Osterkamp and Hedman, 1982). Hence, each bankfull cross-section was characterised by the minimum width-to-depth ratio (Pickup and Warner, 1976) and, as higher breaks-of-slope occur in the cross-sectional profiles, provided a replicable and conservative measure of w_b.

Bankfull cross-sectional area (A) was measured in the GIS as the area bounded by the multibeam sonar river bed and the horizontal line defining w_b (Fig. 3, Table 3). The slope of the river bed (S) was measured from the multibeam sonar data (Fig. 2, Table 3); as many inter-pool bed slopes were adverse, S is the average slope of the reaches up-river of each cross-section.

Calculating a palaeodischarge range from channel morphometry and observed bed sediment calibre

From the morphometric parameters, palaeodischarge was calculated from Eqn 3, 4, 5 and 11 (Table 1). In applying Eqn 11, to account for the large maximum calibre (~500 mm) but heterogeneity of channel forming sediments (sands, gravels, cobbles and boulders) observed during bridge construction across the Lower Suir (e.g. Phillips et al., 2012), three values of n (0.05, 0.03 and 0.01; Acrement, 1989) were used, validated with Eqn 8. Independent checks of V_{cr} and the results of all procedures are presented in Table 3. Results are checked against: (1) Eqn 12 and 5 (Table 1); (2) observations that flow velocities in jokulhlaups range from 5 – 15 $m.s^{-1}$ (Björnsson, 2010), peaking at 20 $m.s^{-1}$ (proximal and overspill zones), <10 $m.s^{-1}$

(distal sandar) and <15 $m.s^{-1}$ (flow convergences) (Maizels, 1993); (3) the minimum flow velocity derived from the Hjulstrom curve required to maintain transport of 100 mm cobbles (~$1m.s^{-1}$; Table 3, V_{100mm}) and 500 mm boulders (~$2m\ s^{-1}$; Table 3 V_{500mm}), and; (4) Eqn 10 (Table 1).

RESULTS

The Long Profile of the Lower Suir

The RIB LP of the lower Suir from Carrick to a point just above its confluence with the Barrow is shown in Fig. 2, with the overlapping reach of the multibeam surveys overlain (GSI 2011a and 2011b). LP is characterised by a sequence of well-defined pools but also some less developed pseudo-pools (Fig. 2). The higher resolution of the multibeam data is apparent, but the fundamental pattern of pools and riffles is the same, especially pool bottom locations and depths, which show minimal difference between surveys. The depth variation of the pool at meander apex 14 is the greatest, probably an effect of the channel splitting around Little Island (Fig. 1) at this point. The greatest difference between the two datasets is in riffle-top depth and form. The stability of pool bottom location and depth confirms that tidal variation was obviated in the RIB survey but also reflects the long-term maintenance of pool-spacing and form by scour (*cf*. Dury, 1970). Pool bottoms in the overlapping survey reach are located where rock is at or very close to the surface and three other pools in the RIB-only survey reach are likewise located where rock is within 1 m of the surface (Fig. 2, indicated by “R”). Of 16 meander apexes, 14 are closely co-located with pools (Fig. 2).

Fig. 2 here.

The regularity of the pool sequence, and the co-location of most meander apexes with pools, could imply a mutual adjustment of channel bedform and planform morphology to discharge (*cf*. Leopold and Wolman, 1957 and 1960; Carling and Orr, 2000). However, the LP and topographic profiles (TPS and TPN) (Fig. 4) appear to have some correspondence, suggesting that the LP could also have inherited some or all its cyclicity from repetitive patterns of relief in the bounding geological topography. Hence, to understand if the LP of the Suir is a hydrological construct or if its form has been inherited from the topographic characteristics of the bounding geological substrate, it is necessary to identify formally any cyclicity within and between the LP, TPS and TPN.

POOL SPACING ALONG THE LOWER SUIR AND ITS GEOLOGICAL-TOPOGRAPHIC CONTEXT

Long Profile (LP)

The ACF plots of dLP (Fig. 5a and b) suggest that the detrended series dLP (d = 1 and d = 2) are mean-reverting but cyclic. Power spectrum analysis (Fig. 5c and d) shows that the peak frequency (accounting for the greatest variance) in dLP (d = 1) = 0.035, equating to a spatial cyclicity (= 1/*f*(*lag*)) of ~1430 m. There are 42 non-random peaks (significant at $p < 0.05$ and $p < 0.01$) in the power spectrum, ranging from 1520 m to 570 m (Fig. 5e). The power spectrum of dLP (d = 2) (Fig. 5d) has no statistically significant peaks (i.e. above the white noise lines at significance levels of 0.05 and 0.01).

Fig. 4 here.

Fig. 5 here.

Topographic Profile South (TPS)

The ACF plots of dTPS (d = 1 and d = 2) are shown in Fig. 6a and b. The detrended series dTPS (d = 1) is mean-reverting but, although oscillatory, is not distinctly cyclic (Fig. 6a). Power spectrum analysis (Fig. 6c) shows that the peak frequency in dTPS (d = 1) = 0.024, equating to a spatial period of ~2080 m. The power spectrum of dTPS (d = 2) (Fig. 6d) has the spectral characteristics of white noise (*p*(random) = 1.0). However, in dTPS (d = 1), there are 8 non-random (significant at $p < 0.05$ and $p < 0.01$) power spectrum peaks (Fig. 6c), ranging from ~2510 to 1860 m (Fig. 6e).

Topographic Profile North (TPN)

The ACF plot of dTPN suggests that the detrended series (d = 1 and d = 2) are mean-reverting and cyclic (Fig. 7a and b). Power spectrum analysis (Fig. 7c) shows that the peak frequency in dTPN (d = 1) = 0.026, equating to a spatial period of ~1900 m. The power spectrum of dTPN (d = 2) (Fig. 7d) has the spectral characteristics of white noise (*p*(random) = 0.75). The power spectrum of dTPN (d = 1) has 74 non-random (significant at $p < 0.05$ and $p < 0.01$) peaks (Fig. 7e), ranging from ~9080 to 1240 m.

Fig. 6 here.

Fig. 7 here.

ACF-CCF and Granger causation analyses

Comparison of the d = 2 elevation series (Fig. 5) shows that the regions of most intense change in dLP (d = 2) located from ~50-100, ~275-400 and ~500-700 lags, correspond with the regions of most intense topographic change in dTPN (d = 2) and dTPS (d = 2). The d = 2 ACF plots shows that this correspondence is governed by both internal autocorrelation and bivariate correlation. Overlaying the d = 1 ACF plots (Fig. 8a and c) confirms that dLP and dTPN display (i) statistically significant cyclicity at a wider range of lags than dTPS but that (ii) the pairwise d = 1 ACF plots show that the periodicities of dTPS and, especially, dTPN have a correspondence with dLP in both direction and magnitude. Plotting the pairwise ACF plots of the d = 2 elevation series shows the correspondence between the curves with the effect of autocorrelation more completely removed (by d = 2 differencing) and indicates corresponding patterns of elevation change in dLP and both dTPS and dTPN (Fig. 8b and d), with an especially close and persistent correspondence between dLP and dTPN (Fig. 8d).

The CCF of the d = 2 elevation series describes the strength, direction (positive to negative) and lag shift of each pairwise association. The CCF plot of dTPS (d = 2) and dLP (d = 2) (Fig. 8e black curve) show significant cross-correlations, oscillating between positive and negative, with a negative lag of 26 - 28 units (1300 – 1400 m). This oscillation between positive and negative correlation is a consequence of a similar oscillation in the ACF of dTPS (d = 2). The negative lag means that dLP leads dTPS. However, it is inconceivable that this means that LP causes TPS; rather, it reflects the repeating spatial sequence of LP with the most powerful 8 significant waveforms (of 42) having spatial periods ranging from 1400 – 1430 m and together

explaining 24 % of the variance accounted for by significant spectral peaks. The CCF plot of dTPN (d = 2) v dLP (d = 2) (Fig. 8f black curve) shows significant positive cross-correlation at +12 and +14 lags and negative cross-correlation at +13 and +21 lags. Hence, dTPN leads dLP by 600 – 1050 m in spatial sequence with an oscillating direction of correlation. Judging by the overlaid ACF plots of dTPN (d = 1) and dLP (d = 1) (Fig. 8c), this lag shift is persistent between ~20 - ~110 lags, beyond which dLP (d = 2) leads dTPN (d = 2). This lag-lead changeover represents the consistently narrow range of the cyclicity in dLP (d = 1) at all lags but the lengthening of significant spatial cycles in dTPN (d = 2) with increasing lag (especially at lags >110). This lengthening causes dTPN (d = 2) to change from leading to lagging dLP (d = 2).

Although the CCFs confirm the existence of statistically significant spatial associations between the LP and the bounding topography, the pairwise tests for Granger causality show that LP is not better predicted by both its own ACF and the inclusion of either TPN or TPS than by its own ACF alone. TPN is the dominant topographic element with respect to having any potential predictive influence on the form of the LP but its explanatory power is not statistically significant. Overall, TPN and TPS do not show significant Granger causality of LP and, therefore, are not useful as predictors of LP. This remains the case even between meander apexes 10 and 16, which define the LP reach that crosses the geological-topographic undulations most nearly orthogonally (Fig. 2 and Table 2).

d = 1	F	F (critical)	p-value	DF

LP = f(TPN)	0.754	1.128	0.386	744
LP = f(TPS)	0.685	1.127	0.408	757
d = 2				
LP = f(TPN)	0.19	1.128	0.663	744
LP = f(TPS)	0.0007	1.127	0.979	757
d = 1				
LP = f(TPN_{10-16})	0.83	1.16	0.36	488
LP = f(TPS_{10-16})	0.31	1.16	0.58	489

Table 2. Results of the Granger causality F-tests and t-tests; TPN_{10-16} and TPS_{10-16} refer to the geological-topographic profiles constraining the reach between LP pools at meander apexes 10-16. F is subcritical in all cases. Interpretation of the test statistics: LP is not better forecast if history of TPS is used (H_0 not rejected); LP is not better forecast if history of TPN is used (H_0 not rejected).

PALAEODISCHARGE FROM POOL-SPACING AND RELATED MORPHOMETRY

Palaeoflow w_b and A

Calculated and measured values of w_b showed good agreement. With pool-spacing represented by the LP power spectrum peak of ~1430 m wavelength, calculated values of w_b are 470 m (Eqn 1) and 190 m (Eqn 2). By comparison, measures of $\underline{w_b}$ from the GIS (multibeam bathymetry and EU-DEM topography) ranged from ~270 - 480 m (Table 3). Measures of *A* from the GIS ranged from ~2610 – 7500 m^2.

Cross-section	w_b (m)	A (m^2)	S	Q_{bf} ($m^3.s^{-1}$)	Q_m (Eqn 3)	Q_m (Eqn 4)	V = Q_{bf}/A ($m.s^{-1}$)	P_w (m)	R (m)	V_{cr} n=0.05	V_{cr} n=0.03	V_{cr} n=0.01	Q_i n=0.05
1	278	3809	0.0009	11975	343	268	3.1	410	9.3	2.6	4.4	13.2	10019
2	287	4371	0.0009	14145	362	282	3.2	383	11.4	3.0	5.0	15.1	13197
3	335	7498	0.0009	27176	472	357	3.6	485	15.5	3.7	6.2	18.5	27744
4	299	3221	0.0009	9776	389	300	3.0	306	10.5	2.9	4.8	14.3	9212
5	271	2782	0.0009	8188	328	258	2.9	320	8.7	2.5	4.2	12.6	7000
6	375	4558	0.0009	14880	572	425	3.3	458	10.0	2.8	4.6	13.8	12555
7	330	2614	0.0009	7593	460	349	2.9	449	5.8	1.9	3.2	9.6	5028

8	332	2779	0.0009	8177	465	353	2.9	406	6.8	2.1	3.6	10.7	5957
9	372	5838	0.0009	20076	565	420	3.4	507	11.5	3.0	5.1	15.2	17732
10	350	3251	0.0009	9886	509	382	3.0	464	7.0	2.2	3.6	10.9	7079
11	356	5982	0.0009	20677	524	393	3.5	657	9.1	2.6	4.3	13.0	15525
12	318	4159	0.0009	13319	432	330	3.2	420	9.9	2.7	4.6	13.7	11418
13	403	4159	0.0009	13319	647	475	3.2	594	7.0	2.2	3.6	10.9	9052
14	469	3845	0.0030	17062	839	437	4.4	552	7.0	4.0	6.7	20.0	15377
15	359	3796	0.0030	16800	531	289	4.4	491	7.7	4.3	7.1	21.4	16280
16	484	3637	0.0030	15952	885	458	4.4	596	6.1	3.7	6.1	18.3	13311

Table 3. Channel morphometric values and calculated discharge, with validation through independent velocity estimates. Mean Q_i = 12280 $m^3.s^{-1}$, standard deviation (SD) = 5658 ($m^3.s^{-1}$); 1 SD range = 17938 – 6623 $m^3.s^{-1}$.

Measuring L_m, s, w_b, A, and S and calculating palaeodischarge to validate palaeodischarge estimates from pool-spacing

Meander wavelength (L_m) and channel sinuosity (s)

Calculated values of L_m based on w_b (~190 m and 470 m) derived from pool-spacing ranged from ~1910 – 4780 m (Eqn 13, range midpoint = ~3340 m) and ~2330 – 5820 m (Eqn 14, range midpoint ~4078 m). L_m, calculated using the measured range of w_b from the GIS (~270 – 480 m, Table 3) ranged from ~2770 – 4950 m (Eqn 13, range midpoint ~3860 m) and ~3380 – 6040 m (Eqn 14, range midpoint ~4700 m). Values of L_m measured from the GIS ranged from 2090 – 4710 m, with a median of 3050 m (Fig. 2). Hence, there is good agreement between the calculated and measured L_m values, with all midpoint values of the calculated ranges (3340 m, 3860 m, 4080 m, 4700 m) falling within the range of measured values (2090 – 4710 m). The ratio of dominant LP cyclicity, representing pool-spacing of 1430 m, to the mid-range values of calculated L_m (3340 m to 4700 m, Eqn 13 and 14) is 0.36 and to the median value of measured L_m (3050 m) is 0.47.

Classified according to bedrock substrate (Table 4; see also Fig. 1 and 2 and Appendix, Section D, Fig. A2), the highest reach-scale value of *s* is 1.2, occurring along channel reaches characterised by consecutive pools scoured into a substrate of Ordovician metasediments (slate, shale, schist) and rhyolite (pools at meander apexes 12 to 16). Along the till-mantled limestone reach (pools at apexes 1 to 4), *s* = 1.05, diminishing to 1.02 in the absence of the till mantle along the bend of meander apex 5. Channel reaches characterised by a substrate of Old Red Sandstone/conglomerate (ORS) are the least sinuous, with mean *s* = 1.005. Where bedrock contacts intersect the channel, *s* generally increases (Table 4). Meander bends developed along limestone shale/limestone/ORS contacts (pools at meander apexes 7 and 10, mean *s* = 1.15) or along the ORS/slate-shale/slate-schist/rhyolite contact around the pool at meander apex 11 (*s* = 1.02) are characterised by significantly greater *s* than the value for the intervening ORS reaches (1.0005 to 1.009) (Appendix Fig. A2).

Reach	**Bedrock**	**Substrate**	***Sinuosity (s)***	**Location (meander apex pool)**
	Limestone	Till-mantled	1.05	1 to 4
	Limestone	Bedrock scoured	1.02	5
	ORS	Till-mantled	1.0005	For 1.2 km down-river of 7
	ORS	Bedrock scoured	1.009	For 2.6 km down-river of 9
	ORS	Bedrock scoured	1.004	For 1.9 km down-river of 10
	Slate-shale/Slate-schist/rhyolite	Bedrock scoured	1.2	12 to 16
Bedrock contact				
	Limestone/limestone shale	Till-mantled	1.06	6
	Limestone shale/ORS	Till-mantled	1.09	7
	Slate/rhyolite	Till-mantled	1.2	8
	Rhyolite/ORS	Bedrock scoured	1.005	9
	ORS/limestone shale/limestone	Bedrock scoured	1.2	10
	ORS/slate-shale-schist/rhyolite	Bedrock scoured	1.02	11

Table 4. Channel sinuosity (*s*) classified by channel substrate.

Calculating V_{cr}

From Eqn 9, mean V_{cr} (Table 3) was 2.9 m.s^{-1} (n = 0.05), 4.8 m.s^{-1} (n = 0.03) and 14.4 m.s^{-1} (n = 0.01). Although all mean values of V_{cr} are within the ranges of Maizels (1993) for jokulhlaups, the peak V_{cr} values associated with n = 0.01 (Table 3) appear excessive. From the Hjulstrom curve, transporting velocities for grain sizes of 100 mm range from 1 – 3.5 m.s^{-1} and for 200 mm fractions from 2 - 6 m.s^{-1}. Hence, although V_{cr} for n = 0.03 is consistent with the values expected from Hjulstrom curve, the Eqn 10 value of V_{cr} = 2.69 m.s^{-1} ((d = 250 mm) suggests that Manning's V_{cr} based on n = 0.05 is the most reliable estimate of V_{cr} involving channel morphometric parameters (Table 3). Hence, only V_{cr} for n = 0.05 will be used in the calculation of instantaneous palaeodischarge (Q_i) from Eqn 11.

Calculating Q_m, Q_{bf} and Q_i

From Eqn 3 based on measured w_b, average Q_m was 520 m^3.s^{-1} (~340 – 890 m^3.s^{-1}). From the range of calculated values of w_b, based on pool-spacing (190 – 470 m), Q_m ranged ~170 - 830 m^3.s^{-1} (range midpoint = 500 m^3.s^{-1}). Incorporating measured bed slope *via* Eqn 4, average Q_m was ~360 m^3.s^{-1} (involving w_b from measured GIS cross-sections) and ~340 m^3.s^{-1} (involving mean S from Table 3 and w_b calculated from pool-spacing, i.e. 190 – 470 m).

Calculated $Q_{1.5}$ (Eqn 7) ranged from 2540 m^3.s^{-1} to 4980 m^3.s^{-1}. Calculated mean Q_{bf} (Eqn 5, using the measured values of A and S in Table 3), was 14300 m^3.s^{-1} (range 7590 – 20670 m^3.s^{-1}), with a standard deviation of 5320 m^3.s^{-1} and 1σ limits of 9000

$m^3.s^{-1}$ and 19630 $m^3.s^{-1}$. Q_{bf} (Eqn 6) ranged from 3620 $m^3.s^{-1}$ (using the mean of the measured values of L_m, 3040 m) to 7990 $m^3.s^{-1}$ (using the midpoint values of L_m involving w_b measured from the GIS, 3860 m and 4080 m). Mean Q_i (Eqn 11, using values in Table 3) was 12280 $m^3.s^{-1}$ with 1σ limits of 6620 $m^3.s^{-1}$ and 17940 $m^3.s^{-1}$. Hence, predictions of Q_{bf} based on L_m are up to one order of magnitude lower than predictions of Q_{bf} involving A and V_{cr} but higher, by one order of magnitude, than both estimates of Q_m.

SUMMARY AND IMPLICATIONS OF THE SERIAL STATISTICS AND PALAEODISCHARGE CALCULATIONS

LP, TPS and TPN are inherently periodic (Fig. 5 – 8). LP is dominated by cyclicity of ~1430 m, which describes the physical pool-to-pool separation. The plot of all waveforms significant at $p < 0.01$ plus the linear trend of LP, usually removed by d = 1 differencing, shows that the LP can be essentially replicated by a FFT model (Fig. 5f grey curve) composed of only its four most significant power spectrum peaks (Fig. 5c). There is overlap in the scale of statistically significant cyclicity between the LP and TPN but not between LP and TPS. However, the influence of all periodic elements in the series, not only statistically significant peaks, causes the LP to have statistically significant lagged cross-correlation with both TPS and TPN. Despite this, the bivariate tests for Granger causality show that neither TPS nor TPN add significant information useful in understanding the cyclicity of LP beyond its own ACF. Most likely, this is because there is no overlap of statistically significant spatial periods in the power spectra of LP and TPS and only a very narrow range of statistically significant periodicities shared by LP and TPN. Hence, although an interpretation based purely on inheritance from topographic variation in the

geological substrate would be a parsimonious explanation of the cyclicity in the LP it would ignore the fact that, if inheritance from TPN to LP has operated, most available signal from TPN is not evident in the LP (Table 2). In summary, therefore, LP shares only a very narrow range of statistically significant power spectrum cyclicity with TPN and none with TPS. Accordingly, TPN and TPS do not show significant Granger causality of LP and, consequently, cannot be considered useful predictors of LP. Although geological topography is not a significant predictor of LP cyclicity, there is a relationship between bedrock substrate and channel plan-form morphology. In general, meander curvature is accentuated where bedrock contacts intersect the channel. Channel reaches developed in the ORS are noticeably straighter than other reach types (Fig. 1) and no meander apexes have developed where ORS is the only substrate. Instead, the straight ORS reaches are bounded by meander bends that have developed across bedrock formation boundaries, with the meander apex occurring in the adjoining non-ORS bedrock type (Appendix Fig. A2).

Interpreting the pool-spacing as a morphological product of palaeodischarge has been validated by a range of other morphological indices and associated palaeodischarge estimates. Present mean discharges of the Suir are on the order of 10^1 $m^3.s^{-1}$ and maximum annual discharge has not exceeded 390 $m^3.s^{-1}$ since 1953 (OPW, 2016). All calculations of discharge based on channel parameters (Q_m, $Q_{1.5}$, Q_{bf}, Q_i) are significantly greater than present discharges: Q_m 10^2 $m^3.s^{-1}$; $Q_{1.5}$ 10^3 $m^3.s^{-1}$; Q_{bf} 10^3 - 10^4 $m^3.s^{-1}$; Q_i 10^3 - 10^4 $m^3.s^{-1}$. However, Q_{bf} and Q_i correspond closely to independent palaeodischarge estimates 1 – 2 x 10^4 $m^3.s^{-1}$ for the submerged palaeochannel beyond Waterford Harbour (Gallagher, 2002; Gallagher et al., 2004). In conclusion, therefore, although there is some geologic-topographic

inheritance within the LP, given the scale of pool-spacing and the present low magnitude discharge regime of the system it is concluded that the dominant influence in determining the pool-spacing of the lower Suir was palaeodischarge. Initial results from research on the River Barrow indicate that its pool-spacing is 800 m (online Appendix, Section E). Therefore, a similarly large palaeodischarge is indicated for that channel, suggesting that the combined palaeodischarge into Waterford Harbour from the Suir-Barrow system was ~15000 - 20000 $m^3.s^{-1}$. However, despite the palaeoenvironmental significance of the pool sequence of the Suir representing extreme palaeodischarge, the questions of why the LP appears to be a filtered subset of the bounding topographic spectrum and, hence, why so much available long wavelength signal from TPS and TPN is not apparent in the cyclicity of the LP (Fig. 2, Table 2) need to be considered, incorporating insights from the palaeohydrology.

Fig. 8 here.

DISCUSSION

Process-form interactions in long profile development and insights from the lower Suir.

In comparison with alluvial beds, more resistant bedrock or coarse clastic substrates are characterised by steeper reach-scale gradients, greater hydraulic roughness and higher stream power, mutually adjusted through an amplifying positive feedback between stream power and gradient but a dampening negative feedback imposed by bed roughness (Goode and Wohl, 2009). Preservation of bedrock or coarse clastic

bed topographic forms produced in extreme flows is enabled by a rapid decrease in both discharge (Baker, 1984) and stream power below high threshold competence (O'Connor et al., 1986). This is an especially important consideration in systems like the Suir that underwent step-changes in the magnitude and frequency of discharge in the transition from a glaciofluvial to a temperate alluvial regime. Consequently, because bedrock or coarse clastic bedforms are produced by, and adjusted to, only high magnitude flows, their pool-spacing exceeds those of alluvial channels (Wohl, 1998). This is consistent with the conclusion of Keller and Melhorn (1978) that, in relation to channel width, the pool-spacing of alluvial and bedrock rivers is the same. This scaling invariance reflects the fundamental control of discharge, rather than boundary material type, on pool-spacing, *via* the positive correlation between discharge and channel width. Dury (1970) also noted the long-term stability of bedforms over a long bedrock reach (~50 km), finding no significant change in either maximum pool depth or depth over riffles recorded in surveys completed over a century apart. Instead, only a redistribution of bedload in pools occurred, sand to pebble-gravel size fractions generally being flushed-through the system (*cf*. Baker and Pickup, 1987). Present day analogues can be seen where pool spacing is adjusted to differing channel width *via* the discharge-width to meander wavelength relationship (Soar and Thorne, 2001), over channel boundaries of differing resistance. Similarly, the co-location of meander apexes at pools along the lower Suir, represented by the 0.47 ratio of the peak LP cyclicity of 1430 m to median L_m (3050 m), accords with the consensus that pool-spacing approximates $L_m/2$ (Leopold et al., 1964; Keller and Melhorn, 1978). In relation to stable alluvial channels, Schumm (1967) concluded that, in addition to discharge, the other independent variable determining L_m is sediment load type, particularly the balance between the

sand-gravel and silt size fractions. In a palaeochannel, the parameters of which do not dominantly reflect active ranges of discharge, some of the past influence of sediment load might also be expressed through channel margin resistance. Considering resistance-form relationships, Hack (1965), Tinkler (1971) and Kennedy (1972) concluded that, as channel resistance increases so too does formative discharge, the net consequence being wider channels with longer L_m. However, channel w:d and L_m have been observed to diminish with increasing channel boundary resistance (Braun, 1983; Harmar and Clifford, 2007). Abrahams (1985) reasoned that along channels of mixed boundary resistance, the varying return interval of formative discharge, as a consequence of changing resistance, dominates variation in L_m. As discharge scales positively with return interval, L_m becomes positively correlated with rock hardness *via* the greater recurrence interval and threshold magnitude of formative discharge in increasingly resistant channel reaches. More generally, Wohl (1998) emphasised the importance of hydraulic control together with downstream variation in substrate resistance imposed by geology. This insight is applicable in the case of the lower Suir and helps to explain the role of channel resistance in bed scour and the variation of s and L_m.

Along the lower Suir, 11 pools are scoured into the bedrock floor of the valley (Fig. 2, pools marked “R”). The median along-path spacing of the consecutive bedrock pools at meander apexes12 to 16 (Fig. 2) is ~1490 m, scoured into slate and rhyolite, both interbedded with shale and schist (Fig. 1 and 2). This reach median pool-spacing lies between the peak and maximum significant cyclicities of the LP (Fig. 5, 1430 m and 1520 m, respectively). Median L_m in this bedrock-scoured reach is 2900 m. Hence, the reach-specific ratio of median pool-spacing to median L_m is 0.49 (~1:2). This

suggests that the bedrock pools, most likely scoured by powerful flows (*cf*. Keller and Melhorn, 1978), and associated meanders represent a co-genetic, self-organised landform assemblage formed under high discharge.

Considering a relationship between pool-spacing, L_m and channel boundary resistance determined by bedrock type, the ORS is probably the most resistant channel substrate bedrock, on account of its resistance to chemical weathering, the relative thickness of its bedding and its resistance to fracture and the development of thin cleavage plains (although the petrographic and environmental factors that determine bedrock resistance to fluvial erosion are complex). By contrast, although the volcanic rocks are inherently hard, their resistance to erosion can be compromised by the presence of interbedded metasedimentary rocks. In relation to the bedrock substrate, the meander with the longest L_m (4710 m, Fig. 2) is a composite form. It consists of straight ORS reaches between (but not including) the pools at meander apexes 9 to 10 (s = 1.009) and 10 to 11 (s = 1.004) but its apical curvature (s = 1.2) is developed around a complex bedrock contact between ORS, limestone and limestone shale (Fig. 1 and 2, Appendix Fig. A2). The pool at meander apex 10 is scoured into the limestone shale/ORS contact. With respect to meander apexes 8 and 11, the same pattern is evident. Channel curvature develops along the contact between ORS and rhyolite or ORS/rhyolite/slate-schist, s increases along the non-ORS reach and the meander apexes at pools occur in the non-ORS channel substrate. However, although no major pools (i.e. with associated meander apexes) occur with ORS as the only substrate, the cyclicity of the LP is maintained within the ORS reach by the development of a channel deepening (a pseudo-pool) between the pools at meander apexes 9 and 10 (Fig. 2, Appendix Fig. A2).

The LP along the ORS-substrate reach is, therefore, very instructive in showing the relationship between pools, meanders, formative discharge and channel boundary resistance. LP cyclicity is maintained, irrespective of changes in channel substrate and, therefore, boundary resistance. However, meander development is very sensitive to channel resistance, with *s* minimised along reaches having the most resistant substrate (ORS) but maximised, at meander bends, only at major apical pools scoured into less resistant channel substrates (particularly bedrock contacts). Hence, L_m is not a simple function of channel boundary resistance but depends on the longitudinal pattern of *s*, determined by variation in substrate resistance. Overall, the data from the lower Suir suggest that its peak LP cyclicity (1430 m) is independent of channel boundary resistance (cf. Keller and Melhorn, 1978). L_m is a complex function of LP cyclicity and varying channel boundary resistance at catchment scale. Along reaches of uniform (or uniformly varying) channel resistance, the scaling relationship between LP cyclicity, *via* pool-spacing, and L_m most closely approaches the ratio 1:2. However, the stability of LP cyclicity along the lower Suir, irrespective of significant variation in channel resistance, the evidence for self-organised pool development involving bedrock scour and the physical scale of pool-spacing suggest that the LP cyclicity of the lower Suir is dominantly representative of palaeodischarge. In the context of the small size of the Suir catchment, the palaeodischarge associated with the pool-spacing, coherent L_m and associated channel parameters represents discharges and scour impossible to produce in the postglacial environment. The magnitude of these flows is, however, consistent with discharges of stored water, usually associated with jokulhlaups.

In the lower Suir, the spacing of pools and meander apexes reflects formative macroturbulent scour peaking at ~1430 m intervals (and channel width ranging from ~190 – 470 m). However, TPS and TPN include significant cyclicity exceeding 1430 m that is either not replicated in the power spectrum of LP or is not statistically significant within it. Hence, the dominant ~1430 m erosional forms of the LP were not simply superimposed onto an undulatory valley floor that also retained underlying cyclicity inherited from the geological topography. Instead, these findings indicate that the establishment of a channel morphologically adjusted (i.e. *via* pool-spacing and meander wavelength) to large, but chronologically restricted, formative discharges involves the erosion of geologic-topographic cyclic components larger than the scale of dominant macroturbulence, which becomes imprinted into the substrate through longitudinally self-organised scour. With the recurrence of similar discharges through an eroding channel, the development of dominant cyclicity in a long profile reflects the establishment of equilibrium mediated by negative feedbacks between the scale of macroturbulence and the changing cyclicity of long profile form through erosion. Judging from the lower Suir, in a glacial context of rising or peak glaciofluvial discharges, L_m would increase with discharge. However, the rate of increase would be inversely related to channel boundary resistance at a given discharge, leading to some modulation of the palaeodischarge signal in the LP by variable channel boundary resistance, especially along geologically complex valleys. Subsequently, in a deglaciated, temperate context (as in the lower Suir), as formerly glaciofluvial channels become paraglacial alluvial systems in interstadial and interglacial environments (cf. Thorp et al. 1997; Glanville et al., 1997; Gallagher and Thorp, 1995; Thorp and Gallagher, 1999), L_m would decrease as discharge diminishes. With postglacial discharges incapable of entraining significant quantities

of available glacigenic sediment (till and coarse glaciofluvial deposits) and exposed bedrock, the LP cyclicity and associated L_m of the late-glacial channel, formed under high discharge, would be preserved. Continuing interglacial evolution of the LP would involve only those channel boundary size-fractions that remain mobile in conditions of reduced discharge. Hence, although long profile cyclicity is dominated by the scale of macroturbulence associated with formative palaeodischarge, the final development of long profile cyclicity and its complementary meander geometry (Fig. 2) represents a balance between geological-topographic inheritance, variability of channel boundary resistance, survival of geological-topographic cyclic modes of a resonant scale to the macroturbulence of the dominant palaeodischarge and post-glacial adjustment of form determined by interactions between diminishing discharge and the paraglacial, inherited, lithological and geotechnical characteristics of the channel (cf. Gallagher and Thorp, 1995).

Glaciofluvial and baselevel context of palaeodischarge variation in long profile development.

Warren and Ashley (1994) interpreted the Barrow valley as a major discharge route of subglacial meltwaters confined between ice sheets that converged in the Irish midlands during the LGM. They also posited a “palaeo-Blackwater” subglacial flow-route, along the large syncline to the north of Youghal (Fig. 1 and Appendix Fig. A4), for the routing of meltwaters from ice in east Cork, south Tipperary and southwest Waterford to the continental shelf west of Waterford Harbour (Appendix Fig. A5). While the inland-to-continental shelf system inferred from the Suir-Barrow-palaeochannel assemblage confirm the prediction of Warren and Ashley (1994) for the discharge route of LGM meltwaters from the midlands, acoustic surveys of the

seabed completed in 2000 by Gallagher (unpublished) and subsequently by the GSI (online Appendix, Section F) have not found any evidence of large discharges on the continental shelf through the “palaeo-Blackwater”. This suggests that meltwaters from ice in east Cork, south Tipperary and southwest Waterford were part of a regional complex of glaciofluvial routeways focused through the lower Suir and Barrow into Waterford Harbour, making it the dominant meltwater conduit of the LGM and early post-LGM period. This palaeo-environmental context suggests that periodic characteristics of the Suir LP represent the superposition of a Holocene system onto an older valley floor that became morphologically adjusted to the interplay between extreme glaciofluvial discharges and the geological foundation. The geological-topographic fabric could not be expressed as a cyclic waveform tied to the plan-form geometry of meanders along the Suir without the mediation of extreme hydrology in the form of very large, high amplitude macroturbulent cells, the dimensions of which determined the longitudinal variability in bed scour.

From the context of the lower Suir and insights gained into the interaction of high discharges and resistant beds (e.g. summarized in Wohl, 1998), it is likely that the initial generation of a sequence of pools, adjusted to high flow erosivity but low bed erodibility (cf. Clifford, 1993), feeds-back into hydrology by influencing spatial variability in stream power, through variation in bed slope and roughness. Consequently, as positive feedbacks become regulated by negative, a fixed sequence of stable pools develops as a form adjusted to the rate of energy expenditure against the channel boundary achieving scour, as opposed to energy expended in overcoming channel boundary resistance (Harmar and Clifford, 2007). Therefore, extreme glaciofluvial discharges impose a hydrologically determined

pattern of macroturbulence, the longitudinal scale of which reflects the scale of the formative discharges. However, the geological-topographic characteristics of the valley floor corresponding in scale with the macroturbulence fix this pattern into a stable spatial configuration. Bedform spacing lengthens as a consequence of increasing discharge. Subsequently, in a context of diminishing post-glacial discharges (as in the lower Suir), the underlying bedform geometry, and its coherent meander planform, are left intact and only superficially draped with Holocene sedimentary bedforms characteristic of alluviation or, in intertidal reaches, tide-dominated flooding. Although the LP of the lower Suir is cyclic it is also extremely flat, with a gradient over 40 km from its tidal limit of only 0.00028. This gradient, however, is an important feature of its raw LP (i.e. not detrended), accounting for 91 % of its variance; the pool-sequence modulates this gradient, suggesting that the formative glaciofluvial discharges occurred within a baselevel context little different from that of the present. Hence, in the context of glacial-to-postglacial channel evolution, long profile development, including both overall gradient and its modulation by cyclic bedforms, is dominantly a product of hydrological controls but includes exogenic factors, especially inheritance of form and materials and the imposition of baselevel. The widest significance of this realisation is that river long profile development closely reflects contextual landscape evolution and the spatial and temporal domains within which its drivers operate.

Quaternary landscape evolution.

Significantly, it is now apparent that glacio-isostatic loading of southeastern Ireland depressed the land surface and increased relative sea level in stadials, with near-field glacio-isostatic transgressions occurring in the presence of calving glaciers at

the end of stadials and in Heinrich Events (Wright and Muff, 1904; Scourse et al., 2009; O'Cofaigh et al., 2012; Gallagher et al., 2015). Hence, glacial-to-interglacial RSL variation has been minimized by glacio-isostatic depression of the Irish crust, e.g. achieving marine transgressions in southeastern Ireland of up to 5 m in the MIS 4-3 transition (Gallagher et al., 2015) when glacio-eustatic sea level was 40 – 70 m lower than present (Siddall et al., 2008). Consequently, it is likely that marine baselevel has consistently been at or above present sea level during the periods of greatest ice sheet melting in interstadials and in the lead up to the last termination (LGM to T1), including the retreat stage bracketed in time by the deposition of the submerged moraine on the continental shelf (Gallagher et al., 2004) and the emplacement of the Blackhall Till limit across the northern part of Waterford Harbour. The entire surveyed LP of the lower Suir shows that the pool-sequence ends at the Blackhall Till limit and Duncannon Bar (Fig. 1), which are spatially coincident. Beyond the Blackhall Till limit and Duncannon Bar, the bed of Waterford Harbour slopes steeply, without a repetitive pool sequence, to the continental shelf. Sub-bottom profiling of the Duncannon Bar (Gallagher, 2000, unpublished – see Appendix, Section G) reveals structures consistent with the form being an ice-contact fan or fan assemblage. The sharp transition in LP gradient at the Blackhall Till limit/Duncannon Bar assemblage, steep on the seaward side but relatively flat landward, suggests that the flat gradient of the lower Suir developed following a rise in RSL post-dating the glacial presence on the continental shelf. However, the steep palaeochannel gradient between the Blackhall Till limit/Duncannon Bar and the submerged moraine further offshore reflects: (1) glacial presence on the seabed during low RSL; (2) glaciofluvial discharges to that ice margin, but; (3) ice margin recession from the submerged moraine to the Blackhall Till limit/Duncannon Bar

(forming the ice-contact fan at this location; Appendix, Section G) either during or prior to a significant increase in RSL. Phase 2 probably also involved a transition from subglacial to proglacial or glacimarine discharges, as the ice margin receded north into Waterford Harbour.

Landward of the Blackhall Till limit/Duncannon Bar, the modulation of the flat gradient of the lower River Suir by the pool sequence of ~1430 m spacing is consistent with: (1) extreme discharges; (2) during high RSL (3) in the post-LGM period; (4) following significant deglaciation of the Irish continental shelf in a context of rising glacio-eustatic sea level, and; (5) continued glacio-isostatic depression of the south of Ireland. The production of extreme glaciofluvial discharges in a context of consistently high RSL explains why the very flat gradient of the lower Suir is modulated by a pool sequence of unexpectedly long wavelength. It probably explains also the locations far inland of the tidal limit of the Suir and the other major rivers of south-east Ireland, as being due to the prevalence of high RSL during the peak epoch of channel formative discharge. Without recent insights to the occurrence of high RSL during glaciation (e.g. O'Cofaigh et al., 2012; Gallagher et al., 2015), paraglacial river channels characterised by a flat gradient modulated by km-scale bedforms would not be predicted; the traditional view has been dominated by predictions of low RSL operating in the presence of ice sheets capable of generating sufficiently large discharges. Inverting this insight suggests that replicate channel studies offer a means of generating important morphogenetic hypotheses that can capture inter-regional complexities in landscape evolution, including identifying the pathways and magnitudes of glaciofluvial discharges to the ocean and improving our

knowledge of the spatial distribution of GIA and consequent styles of RSL change and their effects on channel development.

CONCLUSIONS

Quantitative analyses of the long profile and bounding geological-topography of the lower River Suir have produced several important findings. Fundamentally, the long profile (LP) of the lower River Suir is characterised by a slight gradient modulated by a cyclic sequence of bedforms, mainly pools but including some less developed pseudo-pools, spaced at ~1430 m intervals. Although the geological-topographic substrate bounding the channel of the lower River Suir has an inherent cyclicity, it is dominantly of longer wavelength than the cyclicity of pool-spacing in the LP. Most meander apexes in the lower Suir occur at pools and, therefore, meander wavelength (L_m) is coherent with pool-spacing. This coherence suggests that pool-spacing and L_m have palaeohydrological significance. Accordingly, the pool-spacing and L_m are indicative of mean discharge (Q_m) 2 orders of magnitude greater than present-day values. Similarly, the cross-sectional geometry of the lower Suir reflects formative discharges ($Q_{1.5}$, Q_{bf}, Q_i) 2 - 3 orders of magnitude greater than present. This scale of discharge, combined with similar discharge from the lower River Barrow, are of the same order (10^3-10^4 $m^3.s^{-1}$) as the discharges routed through the submerged palaeochannel south of Waterford Harbour (Gallagher, 2002; Gallagher et al., 2004) but occurred later than, and in a different RSL context from, the flows that incised the submerged palaeochannel.

The preservation of the pool-sequence of the lower Suir is analogous to the preservation of bedrock or coarse clastic bedforms noted by Baker (1984) and

O'Connor et al. (1986) in systems that experienced extreme flows followed by rapid decreases in both discharge and stream power. However, the development of the pool-sequence of the lower Suir reflects a more complex context within which base-level, discharge, sediment supply and hydrological competence evolved. Especially important to understanding the development of the lower Suir LP is the context of glacial to interglacial total environmental change, including changes in the magnitude and frequency of discharge, in the transition from a glaciofluvial to a temperate fluvial regime, and in the context of changing glacio-eustatic sea level and glacio-isostatic RSL. Achieving a better perspective on these interactions provides an improved understanding of landscape as an archive of complex environmental forcing in a climatically and, during the Pleistocene, glacially sensitive part of the North Atlantic Ocean. Hence, this paper provides a template for future research on the many accessible analogous river systems around the formerly glaciated periphery of the North Atlantic Ocean. Carrying out replicate studies of these systems could provide important new insights to Quaternary landscape evolution through the quantitative analysis of channel and valley topography aimed at palaeodischarge reconstruction, the generation of inferences concerning the evolution of palaeodischarge and the untangling of Pleistocene channel development from longer-term valley evolution. The insights from this paper show that the interface between the terrestrial and marine environments can, and should be, bridged and that the dynamism of this interface as a response to glacially-induced environmental changes can provide important insights to Quaternary landscape evolution as a response to climate change and sea level variation. In its regional context, the research presented in this paper demonstrates the complexity of landscape response to deglaciation and RSL change, in particular their modulation of palaeodischarge and hydrological

competence across the last deglacial environmental transition. More broadly, the paper also offers insights to the evolution of channel form in relation to the interaction between channel boundary resistance and the long term evolution of discharge. Hopefully, therefore, the paper can contribute to developing a better understanding of channel form as an important archive of environmental change and landscape response.

ACKNOWLEDGEMENTS

The authors are extremely grateful for the work of two anonymous referees and the editorial team of *ESPL*, whose detailed, constructive reviews contributed significantly to this paper.

The original research for this paper was funded by Enterprise Ireland (Basic Research Grant SC2000/107). Initial ship-time on the Irish Marine Institute vessel RV *Celtic Voyager* was funded by the Geological Survey of Ireland. The authors are sincerely grateful for both funding streams and for the help and care given by the Master and crew of the *Celtic Voyager* and the staff of the Marine Institute. The generosity of the Geological Survey of Ireland, especially Xavi Pellicer of the Quaternary Section, both in making data freely available and providing advice is sincerely appreciated. The RIB sonar survey of the lower River Suir could not have been done without the resources, knowledge, skill and generosity of Arnie Poole, who is owed a deep debt of gratitude. Many thanks to Ivan Pastine (UCD School of Economics) for valuable advice on time series analysis.

References

Abrahams, A.D., (1985) Lithologic control of bedrock meander dimensions in the Appalachian Valley and Ridge Province; a comment, *Earth Surface Processes and Landforms*, 10, 6, 635–642.

Acrement, G.J. (1989). *Guide for selecting Manning's roughness coefficients for natural channelsand flood plains*. V. Series: U.S. Geological Survey water-supply paper; 2339. TC175.A67 1989 627'.4 88-600129

Baker, V.R. (1984). Flood Sedimentation in Bedrock Fluvial Systems, Sedimentology of Gravels and Conglomerates — Memoir 10, *Fluvial Processes*, 87-98.

Baker, V.R. and Pickup, G. (1987). Flood geomorphology of the Katherine Gorge, Northern Territory, Australia, *Geological Society of America Bulletin* doi:10.1130/0016-7606(1987)98<635:FGOTKG>2.0.CO;2

Bayat, E., Rodríguez, J.F., de Almeida, G.A.M. and Saco, P. (2016). Sediment transport, sorting and three-dimensional flow patterns in pool-riffle sequences: Implications for self-maintenance, in: Constantinescu, Garcia & Hanes (Eds), *River Flow 2016*, Taylor and Francis, 1283-1288.

Bernard, J.M., Fripp, J. and Robinson, K. (2007).*Stream restoration design: part 654, national engineering handbook*. U.S. Dept. of Agriculture, Natural Resources Conservation Service, Washington D.C.

Björnsson, H. (2010). Jökulhlaups in Iceland: sources, release and drainage. Iceland in the Central Northern Atlantic: hotspot, sea currents and climate change, May 2010, Plouzané, France.

Box, G. and Jenkins, G. (1970). *Time Series Analysis: Forecasting and Contro*l. San Francisco: Holden-Day.

Bradley, S.L., Milne, G.A., Teferle, F.N., Bingley, R.M. and Orliac, E.J. (2009). Glacial isostatic adjustment of the British Isles: new constraints from GPS measurements of crustal motion, *Geophys. J. Int.* 178, 14–22, doi: 10.1111/j.1365-246X.2008.04033.x

Braun, D.D. (1983). Lithologic control of bedrock meander dimensions in the Appalachian Valley and Ridge Province, *Earth Surf. Proc. Land*., 8, 223-237.

Brooks, A.J., Bradley, S.L., Edwards, R.J. and Goodwyn, N. (2011). The palaeogeography of Northwest Europe during the last 20,000 years, *Journal of Map*s, 573-587.

Carling, P.A. and Orr, H.G. (2000) Morphology of riffle-pool sequences in the River Severn, England, Earth Surface Processes and Landforms, 25, 4, 369-384.

Carlston, C. W. (1965). The relation of free meander geometry to stream discharge and its geomorphic implications, *American Journal of Science*, 263, 864-885.

Clifford, N. (1993). Formation of riffle-pool sequences: field evidence for an autogenetic process, *Sedimentary Geology*, 85(1-4), 39-51. DOI: 10.1016/0037-0738(93)90074-F

Clarke, A., Parkes, M. and Gatley, S. (2007).*The Geological Heritage of Kilkenny. An audit of County Geological Sites in Kilkenny*. Geological Survey of Ireland. Unpublished Report.

Costa J.E. (1983). Paleohydraulic reconstruction of flash-flood peaks from boulder deposits in the Colorado Front Range. *Geol Soc Am Bull*, 94. 8, 986-1004.

Culleton, E.B. (1978) Characterisation of glacial deposits in south Wexford, *Proceedings of the Royal Irish Academy. Section B: Biological, Geological, and Chemical Science*, 78, 293-308. Stable URL:http://www.jstor.org/stable/20519062

de Almeida, G.A.M. and Rodríguez, J.F. (2012). Spontaneous formation and degradation of pool-riffle morphology and sediment sorting using a simple fractional transport model, *Geophysical Research Letters*, 39, L06407, doi:10.1029/2012GL051059.

Dolan, R., Howard, A. and Trimble, D. (1978). Structural Control of the Rapids and Pools of the Colorado River in the Grand Canyon, *Science*, 202 (4368), 629-631. [DOI:10.1126/science.202.4368.629]

Dury, G. H. (1970). A re-survey of part of the Hawkesbury River, New South Wales, after one hundred years, *Australian Geographical Studies*, 8, 121–132.

Dury, G.H. (1976) Discharge prediction, present and former, from channel dimensions. *J. Hydrol.*, 30, 219-245.

EPA (2016). Environmental Protection Agency, Water/Water Framework Directive, Catchments, data available online at http://gis.epa.ie/GetData/Download, last accessed on August 12, 2016.

EU-DEM (2014). Digital Elevation Model over Europe, eudem_dem_5deg_n50w005 and eudem_dem_5deg_n50w010, data available online at http://www.eea.europa.eu/data-and-maps/data/eu-dem#tab-original-data, last accessed on August 12, 2016.

Gallagher, C. (2002). The morphology and palaeohydrology of a submerged glaciofluvial channel emerging from Waterford Harbour onto the nearshore continental shelf of the Celtic Sea, *Irish Geography,* 35, 2, 111-132.

Gallagher, C. and M. Thorp (1997). The age of the Pleistocene raised beach near Fethard, County Wexford, using infra red stimulated luminescence (IRSL), *Irish Geography*, 30(2), 68-89.

Gallagher, C. and Thorp, M. (1995). The Fluvial Concentration of Heavy Minerals in the Slieve Bloom Mountains, Central Ireland, *Irish Geography*, 28, 1.

Gallagher, C., Sutton, G. and Bell, T. (2004). Submerged ice marginal forms in the Celtic sea off Waterford Harbour, Ireland. Implications for understanding regional glaciation and sea level changes following the last glacial maximum in Ireland, *Irish Geography*, 37, 2, 145-165. doi:http://dx.doi.org/10.2014/igj.v37i2.205.

Gallagher, C., Telfer, M. W. and Ó Cofaigh, C. (2015). A Marine Isotope Stage 4 age for Pleistocene raised beach deposits near Fethard, southern Ireland. *Journal of Quaternary Science*. doi: 10.1002/jqs.2808

Geological Survey of Ireland (2011a). Infomar Programme, *RV Keary 2011 Leg 1*, data available online at https://jetstream.gsi.ie/iwdds/map.jsp, last accessed on August 12, 2016.

Geological Survey of Ireland (2011b). Infomar Programme, *RV Geo* 2011 Leg 2 Waterford Harbour surveys, data available online at https://jetstream.gsi.ie/iwdds/map.jsp, last accessed on August 12, 2016.

Geological Survey of Ireland (2015a). Infomar Programme, multibeam bathymetry, cruise CV_07_02, data available online at https://jetstream.gsi.ie/iwdds/map.jsp, last accessed on August 12, 2016.

Geological Survey of Ireland (2015b). 1:100,000 Bedrock Geology, available online at http://www.dccae.gov.ie/natural-resources/en-ie/Geological-Survey-of-Ireland/Pages/Data-Downloads.aspx, last accessed 12 August, 2016.

Geological Survey of Ireland (2015c). Quaternary Geology, available online at http://www.dccae.gov.ie/natural-resources/en-ie/Geological-Survey-of-Ireland/Pages/Data-Downloads.aspx, last accessed 12 August, 2016.

Gilbert, R.O. (1987). *Statistical Methods for Environmental Pollution Monitoring*, Wiley, NY.

Glanville, P., M. B. Thorp, and C. Gallagher. "Bio-climatic change and the response of rivers in Irish upland regions during the Late Quaternary, with particular attention to the upper river Liffey catchment, Co. Wicklow." In: Sweeney, J (ed). *Global Change and the Irish Environment*. Dublin, Royal Irish Academy, 133-141.

Goode, J. R., and E. Wohl (2010), Substrate controls on the longitudinal profile of bedrock channels: Implications for reach-scale roughness, *J. Geophys. Res*., 115, F03018, doi:10.1029/2008JF001188.

Hack, J.T. (1965). *Postglacial drainage evolution and stream geometry in the Ontonagon area*, Michigan. 504-B. Washington, DC: U.S. Geological Survey.

Hammer, Ø., Harper, D.A.T., and Ryan, P.D. (2001). PAST: Paleontological Statistics Software Package for Education and Data Analysis. *Palaeontologia Electronica,* 4, 1, 9pp. http://palaeo-electronica.org/2001_1/past/issue1_01.htm

Harmar, O.P and Clifford, N.J, (2007). Geomorphological explanation of the long profile of the Lower Mississippi River, *Geomorphology*, 84, 222–240.

Hegarty, S. (2004). Limits of Midlandian glaciation in south-eastern Ireland, *Irish Geography*, 37, 1, 60-76. DOI: http://dx.doi.org/10.2014/igj.v37i1.194

Howard, A.D. (1998). Long Profile Development of Bedrock Channels: Interaction of Weathering, Mass Wasting, Bed Erosion, and Sediment Transport. In, Tinkler, K.J. and Wohl, E. (eds), *Rivers Over Rock: Fluvial Processes in Bedrock Channels*, American Geophysical Union Geophysical Monograph Series, 107, doi.org/10.1029/GM107p0133, 323p.

Keller, E. A. and Melhorn, W. N. (1978). Rhythmic spacing and origin of pools and riffles. *Geological Society of America Bulletin*, 89, 723–730.

Kellerhals, R. and Church, M. (1989). The morphology of large rivers: characterization and management, in Dodge, D.P. [ed.] *Proceedings of the International Large River Symposium*, Canadian Special Publication of Fisheries Aquatic Science, 106, pp. 31 – 48.

Kendall, M.G. (1975). *Rank Correlation Methods*, 4th edition, Charles Griffin, London.

Kennedy, B. A. (1972) ''Bankfull' discharge and meander forms', *Area*, 4, 209-212.

Lambeck, K. (1993a). Glacial rebound of the British Isles - I. Preliminary model results, *Geophys. J . Int*., 115, 941-959.

Lambeck, K. (1993b). Glacial rebound of the British Isles - II. A high-resolution, high-precision model, *Geophys. J . Int*., 115, 960-990.

Leopold, L.B. and Wolman, M.G. (1957). River channel patterns - braided, meandering and straight. *US Geol Surv Prof Pap*, 282-B:39-85.

Leopold, L.B. and Wolman, M.G. (1960). River meanders. *Geol Soc Am Bull*, 71, 769-794.

Leopold, L. B., Wolman, M. G. and Miller, J. P. (1964). *Fluvial Processes in Geomorphology*, W. H. Freeman, San Francisco, CA.,

Limerinos, J.T. (1970). *Determination of the Manning coefficient from measured bed roughness in natural channels*. US Geological Survey, Water Supply Paper 1898-B, 47 p.

Lisiecki, L. E., and Raymo, M.E. (2005), A Pliocene-Pleistocene stack of 57 globally distributed benthic d18O records, *Paleoceanography*, 20, PA1003, doi:10.1029/2004PA001071.

Lisle, T. (1986). Stabilization of a gravel channel by large streamside obstructions and bedrock bends, Jacoby Creek, northwestern California, *Geological Society of America Bulletin*, v. 97, p. 999-101.

Maizels, J. (1993). Lithofacies variations within sandur deposits: the role of runoff regime, flow dynamics and sediment supply characteristics, *Sedimentary Geology*, 85, 299-325.

Mann, H.B. (1945). Non-parametric tests against trend, *Econometrica* 13:163-171.

McCabe, A.M. and Dunlop, P. (2006). *The Last Glacial Termination in Northern Ireland*, Geological Survey of Northern Ireland, 93pp.

O'Cofaigh C., Matt W. Telfer M.W, Bailey R.M.,Evans D.J.A. (2012). Late Pleistocene chronostratigraphy and ice sheet limits, southern Ireland, *Quaternary Science Reviews*, 44: 160-179. DOI: 10.1016/j.quascirev.2010.01.011

O'Connor, J.E., Webb, R.H. and Baker V.R. (1986). Paleohydrology of pool-and-riffle pattern development: Boulder Creek, Utah, *Geological Society of America Bulletin*, 97, 4, 410-420.

OPW (2016). Hydro-data, Station: Cahir Park (16009), data available online at http://waterlevel.ie/hydro-data/search.html?rbd=SOUTH%20EASTERN%20RBD#, last accessed on August 12, 2016.

Orme, A. (1964). Planation surfaces in the Drum Hills, County Waterford, and their wider implications, *Irish Geography*, 5, 1, 48-72.

Osterkamp, W. R. & Hedman, E. R. (1982). *Perennial streamfiow characteristics related to channel geometry in Missouri River basin*. US Geol. Survey Prof. Paper no. 1242, Washington, DC.

Parkes, M. & Meehan, R. (2012). *An audit of Geological Sites in Kilkenny (Phase 2), The Geological Heritage of Kilkenny.* Geological Survey of Ireland. Unpublished Report.

Phillips, A., Sibert, B., Eptisa, J.N., Astiz, M.A., Casado, C.F. and Santos, A. (2012). N25 Waterford Bypass Geotechnical Issues and Solutions, *Geotechnics On Irish Roads, 2000 - 2010 A Decade of Achievement*, Geotechnical Society of Ireland, CPD Conference Thursday 11th October 2012.

Pickup, G., and R. F. Warner (1976). Effects of hydrologic regime on magnitude and frequency of dominant discharge, *J. Hydrol*., 29, 51 – 75.

Richards, K.S. (1976). The morphology of riffle-pool sequences, *Earth Surface Processes*, 1, 1,71–88. DOI: 10.1002/esp.3290010108.

Scourse J. D., Haapaniemi A.I., Colmenero-Hidalgo E., Peck V.L., Hall I.R., Austin W.E.N, Knutz P.C., and Zahn R. (2009). Growth, dynamics, and deglaciation of the last British-Irish Ice Sheet: The deep-sea ice-rafted detritus record, *Quaternary Science Reviews*, 28, 3066–3084, doi:10.1016/j.quascirev.2009.08.009Scourse J.D.

Siddall, M., Rohling E.J., Thompson W.G. and Waelbroeck, C. (2008). MIS 3 Sea-level fluctuations: data synthesis and new outlook, *Reviews of Geophysics*, 46. RG4003. 10.1029/2007RG000226

Sklar, L.S., and Dietrich, W.E. (2001). Sediment and rock strength controls on river incision into bedrock, *Geology*, v. 29, p. 1087–1090, doi: 10.1130/0091-7613(2001)0292.0.CO;2

Sklar, L.S., and Dietrich, W.E. (2004). A mechanistic model for river incision into bedrock by saltating bed load, *Water Resources Research*, v. 40, 6**,** 1944-7973**.** doi:10.1029/2003WR002496**.**

Soar, P.J. and Thorne, C.R. (2001). *Channel Restoration Design for Meandering Rivers*. Coastal and Hydraulics Laboratory, US Army Engineer Research and Development Center, Vicksburg.

Student (1908). The Probable Error of a Mean, *Biometrika*, 6, 1-25.

Thorp, M. and Gallagher, C. (1999). Dating recent alluvial sediments in the Wicklow Mountains, *Irish Geography*, 32, 2.

Thorp, M., Gallagher, C. and Glanville, P. (1997). 'Global change and river behaviour' In: Sweeney, J (ed). *Global Change and the Irish Environment*. Dublin. Royal Irish Academy, pp.108-121.

Tinkler, K. J. (1971) 'Active valley meanders in south-central Texas and their wider implications', *Geological Society of America Bulletin*, 82, 1783-1800.

Wald, A. and Wolfowitz, J. (1940), "On a test whether two samples are from the same population," *Ann. Math Statist.* 11, 147-162.

Warren W.P. (1985) Stratigraphy, in, Edwards K.J. and Warren W.P. (eds) *The Quaternary History of Ireland*, Academic Press, London, 39-65.

Warren, W.P. and Ashley, G.M. (1994). Origins of the ice-contact stratified ridges (eskers) of Ireland, *Journal of Sedimentary Research*, A64 (3): 433-449.

Wessa, P. (2016), Free Statistics Software, Office for Research Development and Education, version 1.1.23-r7, URL http://www.wessa.net/, last accessed on August 12, 2016.

Williams, G.E. (1970). The central Australian stream floods of February-March 1967. *J. Hydrol.*, 11, 185-200.

Williams, G.P. (1978). Bank-full discharge of rivers. *Water Resour*. *Res*., 14, 6, 1141-1154.

Williams, G.P. (1983a). Improper use of regression equations in earth sciences. *Geology*, 11, 195-197.

Williams, G.P. (1983b). Paleohydrological methods and some examples from Swedish fluvial environments, I - cobble and boulder deposits, *Geogr Ann*, 65A, 3-4, 227 -243.

Williams G.P. (1984). Paleohydrological methods and some examples from Swedish fluvial environments, II - river meanders. *Geogr Ann*, 66A (1-2), 89-102.

Wohl, E. (1998). Bedrock channel morphology in relation to erosional processes. In: Tinkler, K.J. and Wohl, E. (eds), *Rivers Over Rock: Fluvial Processes in Bedrock Channels*, American Geophysical Union Geophysical Monograph Series, 107, doi.org/10.1029/GM107p0133, 323p.

Wright, W.B. and Muff, H.B. (1904). The pre-glacial raised beach of the south coast of Ireland, *Scientific Proceedings of the Royal Dublin Society*, N.S. 10, 250-324.

Yalin, M. S. (1971). On the formation of dunes and meanders, *Proceedings of the 14th Congress of the International Association for Hydraulic Research*, 3, 101-108.

Yalin, M. S. (1977). *Mechanics of Sediment Transport*, 2nd ed, Pergamon Press, Oxford, 298 pp.

Yalin, M. S. (1992). *River Mechanics*, Pergamon Press, Oxford, 219 pp.

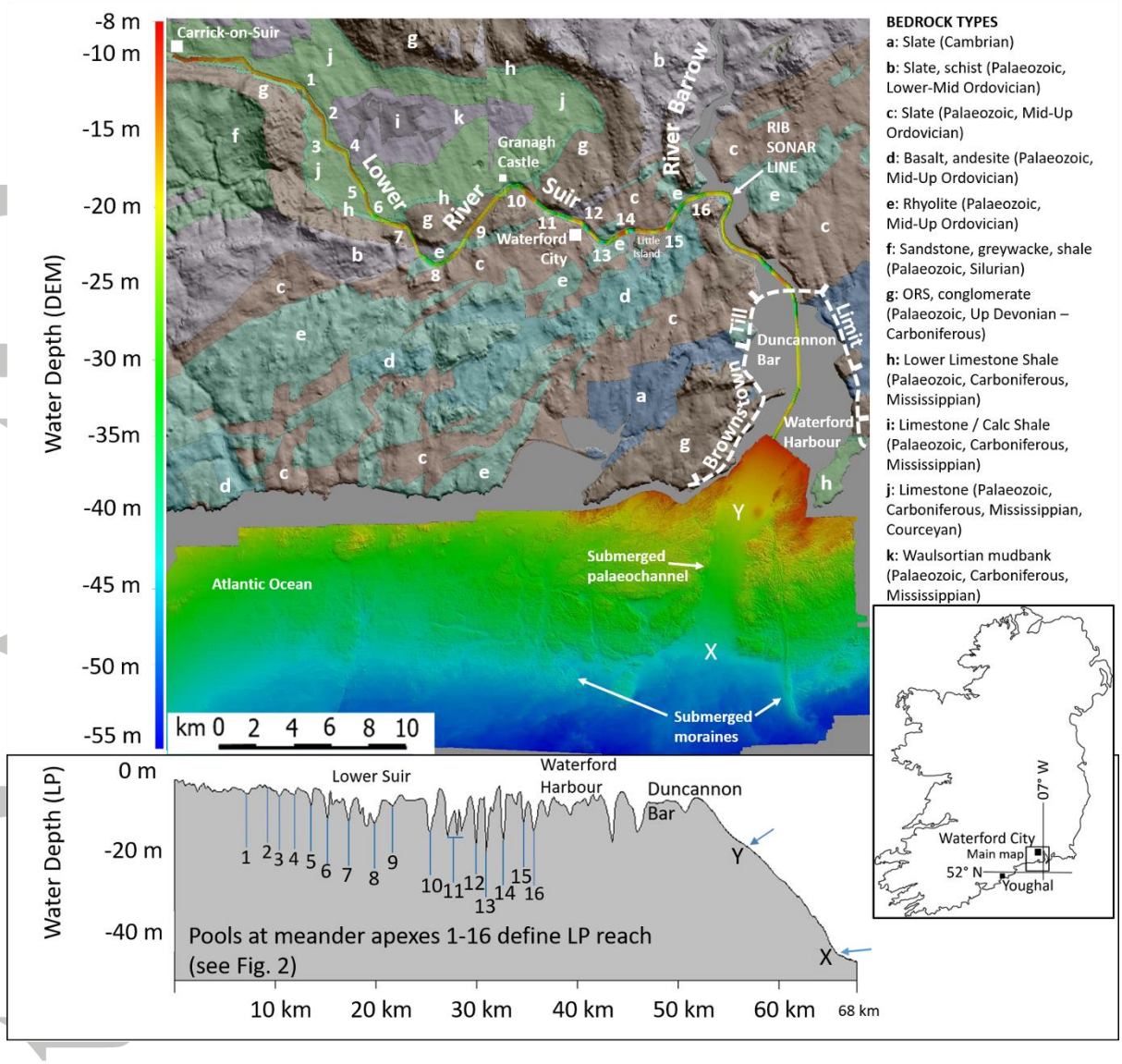

Figure 1. (Upper panel) River Suir catchment, study reach and RIB sonar line extending to offshore palaeochannel. Topographic data: EU-DEM (2014) 25 m/pixel. Bedrock types; Geological Survey of Ireland (GSI, 2015b). Offshore multibeam bathymetry and palaeochannel: Geological Survey of Ireland (GSI, 2015a). RIB sonar line (width not to scale) from Carrick-on Suir through Waterford Harbour to the offshore palaeochannel; original to this paper. Topography vertical exaggeration x 3. Offshore multibeam sonar vertical exaggeration x 10. (Lower panel) Long profile extends from Carrick-on-Suir to the submerged palaeochannel (points X and Y for reference); numbers 1 – 16 show the locations of pools with co-located meander apexes. North is up.

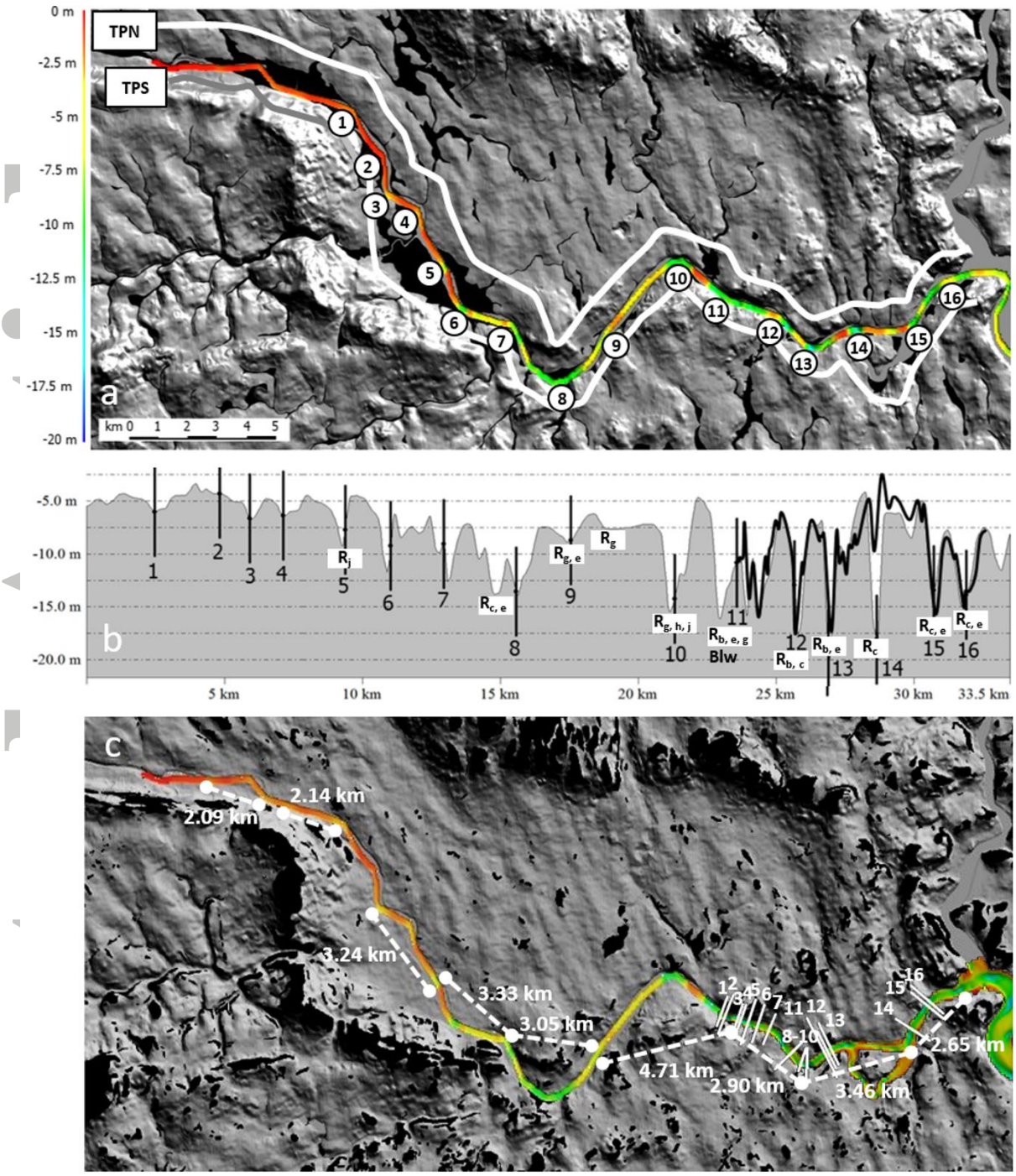

Figure 2. (a) RIB sonar elevation model (width not to scale) of the lower Suir and contextual topography. Pools are numbered. Topographic profiles TPN (north) and TPS (south) are shown as white lines (initial segment of TPS is grey for clarity). Black fills between TPN and TPS, bounding the sonar line, represent alluvium (GSI, 2015c), but outside these regions the topography is dominated by till mantling bedrock or bedrock within 1 m of the surface (panels b and c). Topographic base is

EU-DEM (2014). River depth sounding is original RIB single beam sonar. (b) RIB sonar long profile compared with the long profile plotted from the GSI multibeam sonar datasets (GSI, 2011a and b) along the course of the RIB (heavy black line). Numbered black bars represent meander apexes (see panel a). The confluence of the Kilkenny Blackwater River is marked “Blw” (not the same as the Youghal River Blackwater – see Fig. 1 and online Appendix Fig. 4). “R” represents rock at or within 1 m of the surface, the rock type represented by the subscript: b, slate/schist; c slate; e rhyolite; g Old Red Sandstone, conglomerate; h limestone shale; j limestone (see Fig. 1 for full rock type letter key). (c) Meander wavelengths (km) defined by sequences of three consecutive pool locations (dashed white lines with terminal dots, representative only). Numbered solid white lines show measured cross-sections for identification of bankfull channel (see Fig. 3), using GSI multibeam sonar and EU-DEM topographic model (multibeam data start ~100 m up-river of cross-section 1). Scale as in panel a. North is up.

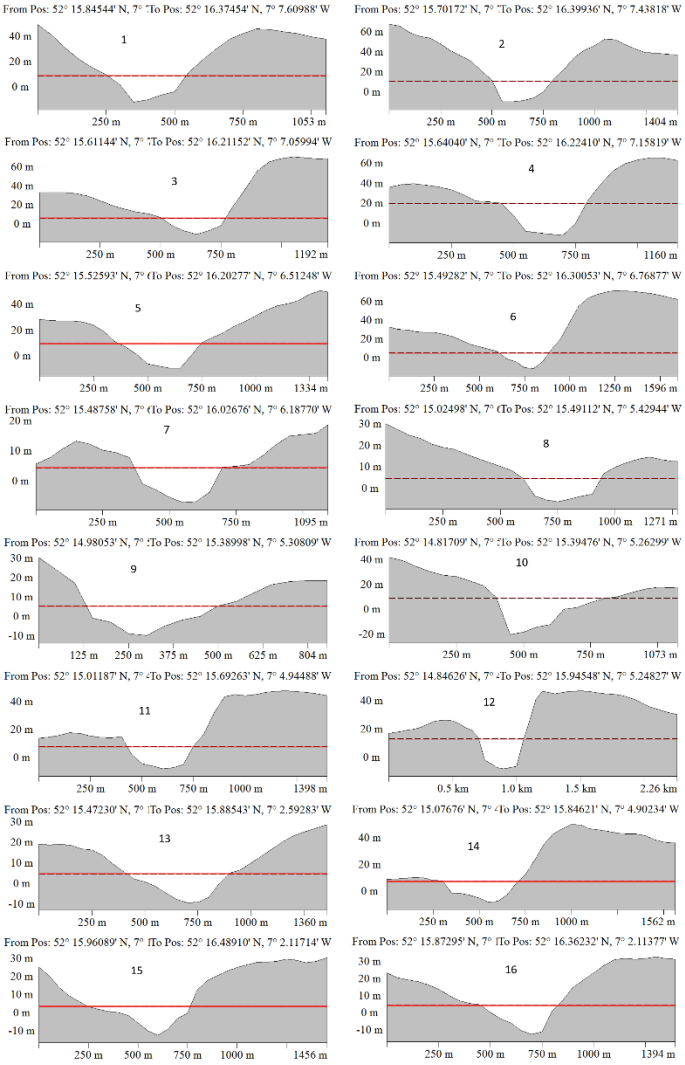

Figure 3. Bankfull channel cross-sections derived from GSI (2011a and b) multibeam sonar and EU-DEM (2014) topographic data (cross-section numbers as in Fig. 2). The cross-sections (the white area between the horizontal line and topographic surface) define the minimum w:d (see text for details).

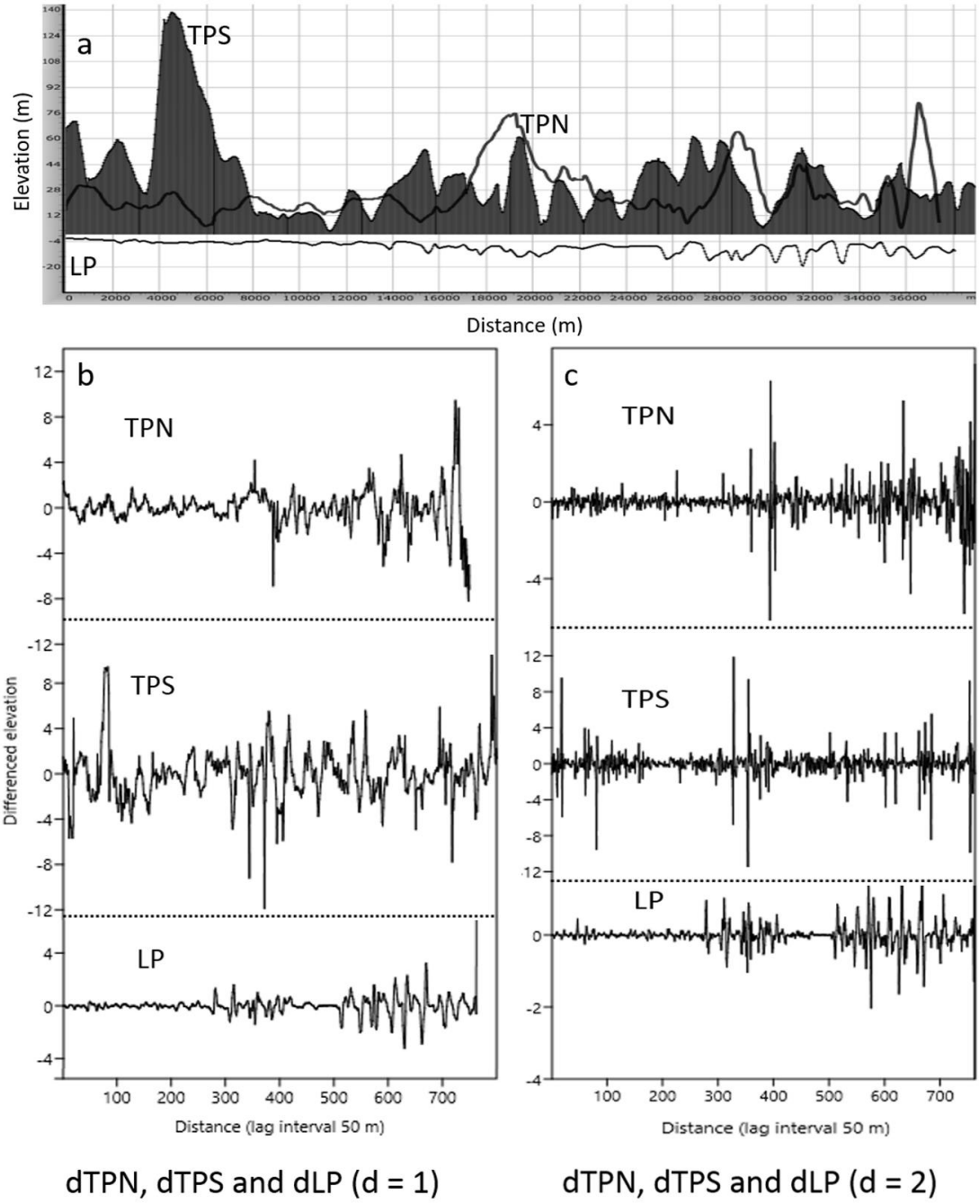

Figure 4. (a). Elevation profiles of the geological topography (EU-DEM, 2014) south (TPS, white profile) and north (TPN, filled profile) of the lower Suir with the long profile (LP) of the Suir (all to the same vertical scale, axes in m). (b) Detrended elevation series (d = 1) dTPS (upper), dTPN (middle) and dLP (lower). (c) Detrended elevation series (d = 2) dTPS (upper), dTPN (middle) and dLP (lower). Distance x 50 m lag spacing.

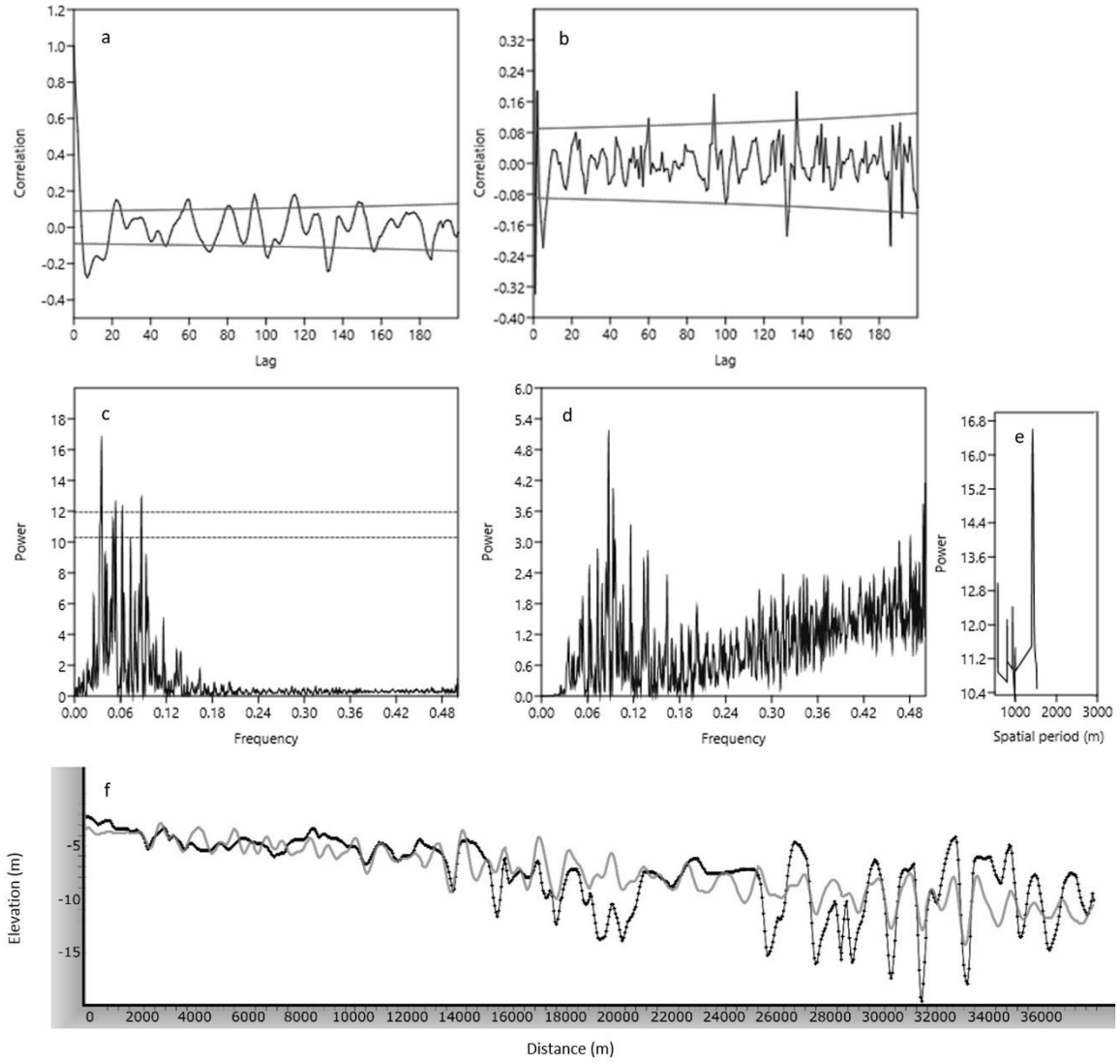

Figure 5. (a) ACF (correlation) plot of dLP (d = 1). (b) ACF (correlation) plot of dLP (d =2). Peaks or troughs outside the upper and lower lines in (a) and (b) are significant at $p > 0.05$. (c) Periodogram of dLP (d = 1). The lower and upper lines are the $p < 0.05$ and $p < 0.01$ (white noise) boundaries respectively. (d) Periodogram of dLP (d = 2); There are no statistically significant peaks in dLP (d = 2) power spectrum. (e) Statistically significant spatial periodicities in dLP (d = 1). The peak frequency (power) has a spatial period of ~1430 m. (f) FFT model (grey curve) of LP (black curve) based only on the 4 periodogram waveforms significant at $p < 0.01$.

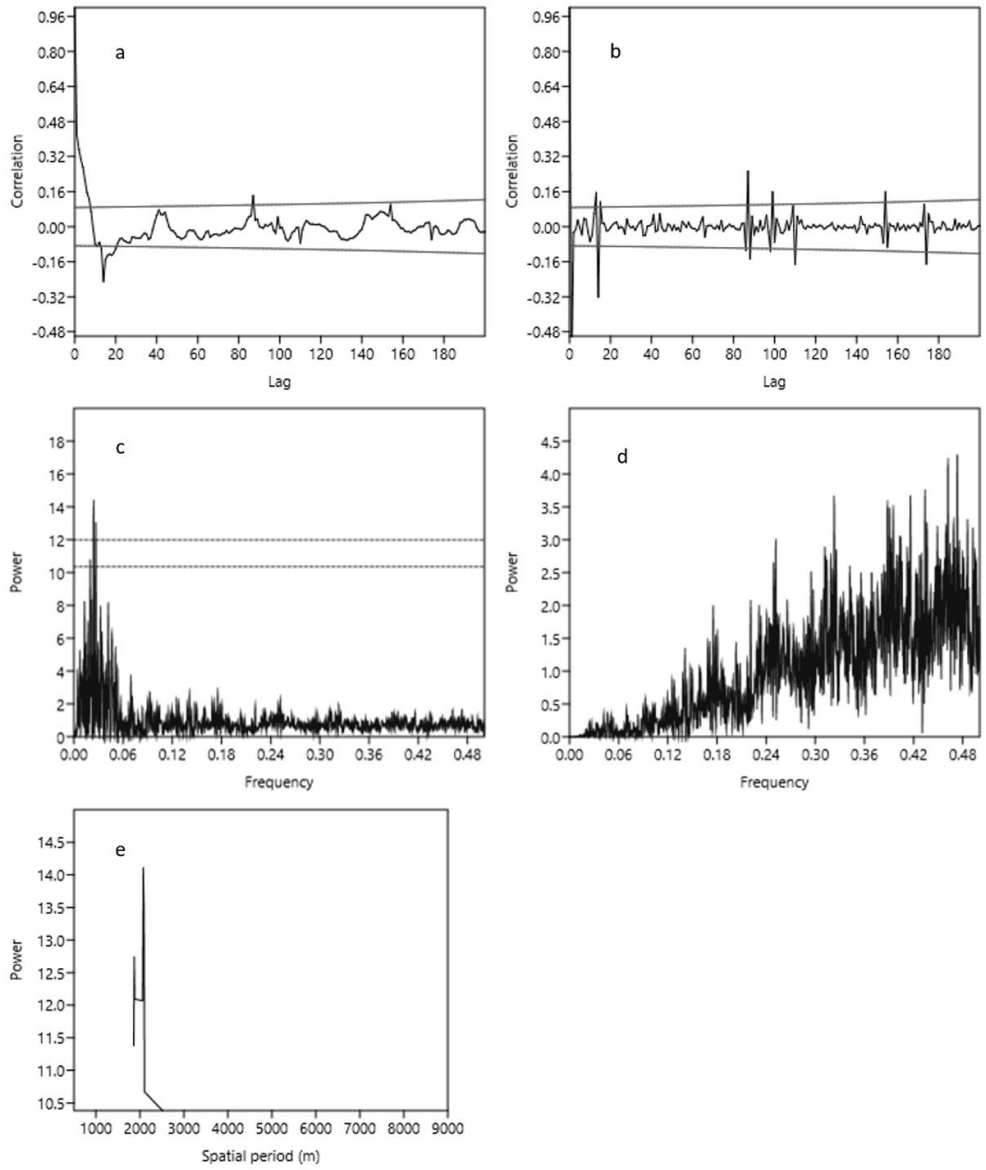

Figure 6. (a) ACF (correlation) plot of dTPS (d = 1). (b) ACF (correlation) plot of dTPS (d = 2). Peaks or troughs outside the upper and lower lines in (a) and (b) are significant at $p > 0.05$. (c) Periodogram of dTPS (d = 1). The lower and upper lines are the $p < 0.05$ and $p < 0.01$ (white noise) boundaries respectively. (d) Periodogram of dTPS (d = 2). There are no statistically significant peaks in this power spectrum. (e) Statistically significant spatial periodicities in dTPS (d = 1). The peak frequency (power) has a spatial period of ~2080 m.

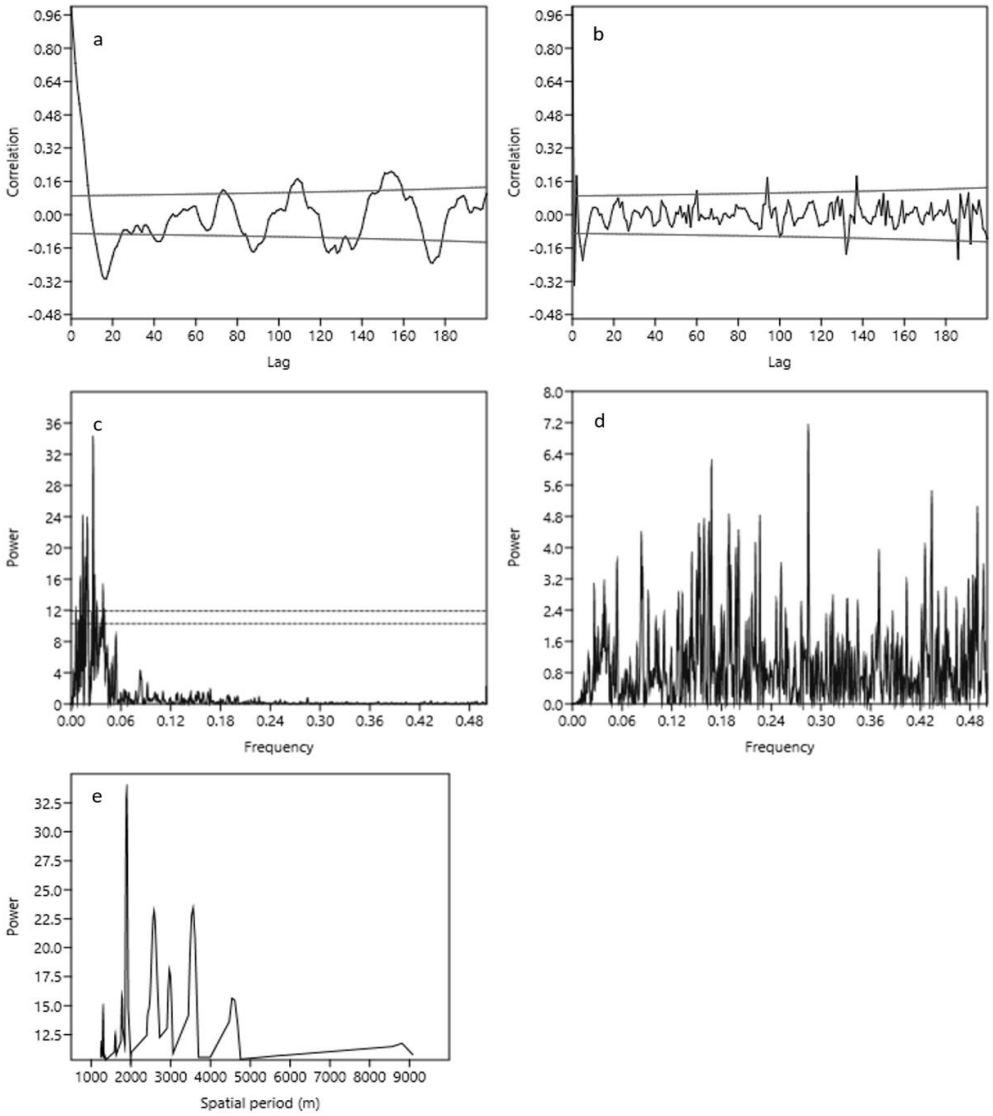

Figure 7. (a) ACF (correlation) plot of dTPN (d = 1). (b) ACF (correlation) plot of dTPN (d = 2). Peaks or troughs outside the upper and lower lines in (a) and (b) are significant at $p > 0.05$. (c) Periodogram of dTPN (d = 1). The lower and upperlines are the $p < 0.05$ and $p < 0.01$ (white noise) boundaries respectively. (d) Periodogram of dTPN (d = 2). There are no statistically significant peaks in this power spectrum. (e) Statistically significant spatial periodicities in dTPN (d = 1). The peak frequency (power) has a spatial period of ~1900 m but a narrow range of significant peaks with spatial periods of ~1350 to ~1500 m exist, providing a physical overlap with the power spectrum peak of dLP (d = 1).

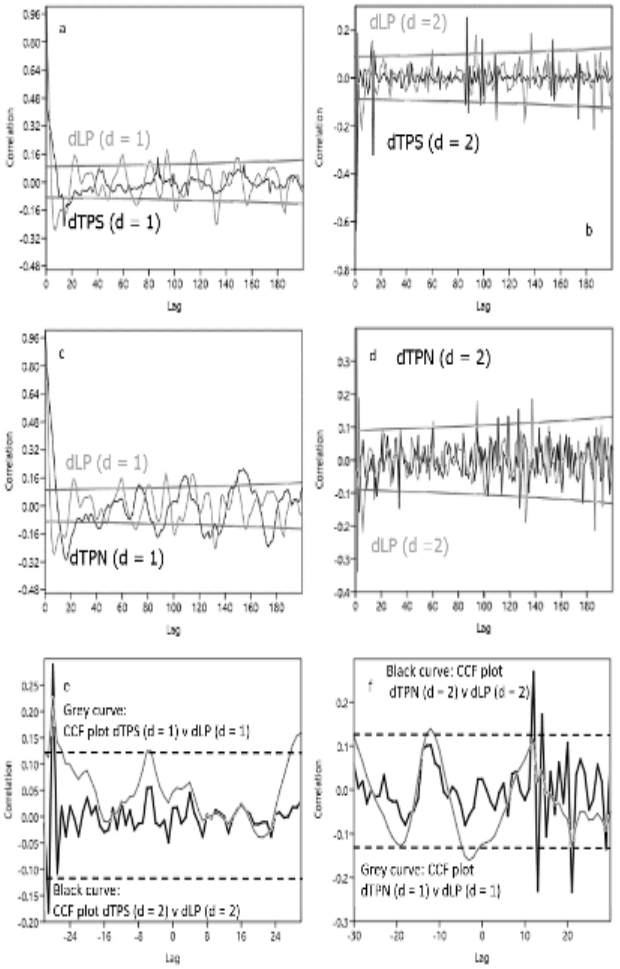

Figure 8. (a) Overlaid ACF plots of dTPS and dLP, d = 1. (b) Overlaid ACF plots of dTPS and dLP, d = 2. Peaks or troughs outside the upper and lower lines in (a) and (b) are significant at $p > 0.05$. (c) Overlaid ACF plots of dTPN and dLP, d = 1. (d) Overlaid ACF plots of dTPN and dLP, d = 2. (e) Grey curve: CCF plot of dTPS (d = 1) v dLP (d = 1). Black curve: CCF plot of dTPS (d = 2) v dLP (d = 2). Correlations exceeding the 95 % confidence interval lie outside the dashed lines (critical value = ±0.11 at the 95% confidence interval). Positive lags: dTPS leads dLP. Negative lags: dLP leads dTPN. (f) Grey curve: CCF plot of dTPN (d = 1) v dLP (d = 1). Black curve: CCF plot of dTPN (d = 2) v dLP (d = 2). Correlations exceeding the 95 % confidence interval lie outside the dashed lines (critical value = ±0.12 at the 95% confidence interval). Positive lags indicate that dTPN leads dLP, negative lags that dLP leads dTPN.